

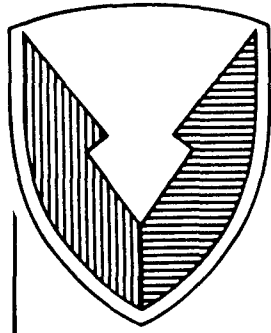
1093

AD 133 33

# R D & E

C E N T E R

## Technical Report



No. 13234

DEVELOPMENT AND MANUFACTURE  
OF A TWO-BOLT CENTERGUIDE FOR  
THE M1 TRACK  
CONTRACT NUMBER DAAE07-85-R-068  
JANUARY 1987

NATHANIEL SMITH  
FMC CORPORATION  
STEEL PRODUCTS DIVISION  
By ANNISTON, AL 36201

APPROVED FOR PUBLIC RELEASE:  
DISTRIBUTION IS UNLIMITED

20030113135

U.S. ARMY TANK-AUTOMOTIVE COMMAND  
RESEARCH, DEVELOPMENT & ENGINEERING CENTER  
Warren, Michigan 48397-5000

REPORT

NOTICES

This report is not to be construed as an official Department of the Army position.

Mention of any trade names or manufacturers in this report shall not be construed as an official endorsement or approval of such products or companies by the U.S. Government.

Destroy this report when it is no longer needed. Do not return it to the originator.

REPORT DOCUMENTATION PAGE

1a. REPORT SECURITY CLASSIFICATION Unclassified		1b. RESTRICTIVE MARKINGS	
2a. SECURITY CLASSIFICATION AUTHORITY		3. DISTRIBUTION / AVAILABILITY OF REPORT Approved for Public Release: Distribution is unlimited	
2b. DECLASSIFICATION / DOWNGRADING SCHEDULE			
4. PERFORMING ORGANIZATION REPORT NUMBER(S)		5. MONITORING ORGANIZATION REPORT NUMBER(S) <b>13234</b>	
6a. NAME OF PERFORMING ORGANIZATION FMC Corporation Steel Products Division	6b. OFFICE SYMBOL (if applicable)	7a. NAME OF MONITORING ORGANIZATION U. S. Army Tank-Automotive Command Attn: AMSTA-RS <b>RVT</b>	
6c. ADDRESS (City, State, and ZIP Code) Anniston, AL 36201		7b. ADDRESS (City, State, and ZIP Code) Warren, MI 48397-5000	
8a. NAME OF FUNDING / SPONSORING ORGANIZATION	8b. OFFICE SYMBOL (if applicable)	9. PROCUREMENT INSTRUMENT IDENTIFICATION NUMBER <b>DAAE07-85-C-R068</b>	
8c. ADDRESS (City, State, and ZIP Code)		10. SOURCE OF FUNDING NUMBERS	
		PROGRAM ELEMENT NO.	PROJECT NO.
		TASK NO.	WORK UNIT ACCESSION NO.
11. TITLE (Include Security Classification) Development and Manufacture of a Two-Bolt Centerguide for the M1 Track (u)			
12. PERSONAL AUTHOR(S) Smith, Nathaniel			
13a. TYPE OF REPORT Final	13b. TIME COVERED FROM July 85 TO Jan 87	14. DATE OF REPORT (Year, Month, Day) 87 Jan	15. PAGE COUNT 65
16. SUPPLEMENTARY NOTATION			
17. COSATI CODES		18. SUBJECT TERMS (Continue on reverse if necessary and identify by block number)	
FIELD	GROUP	Centerguide, Steel Forging, Two-Bolt Concept, Assembly Torque	
19. ABSTRACT (Continue on reverse if necessary and identify by block number)			
This program was initiated to develop a two-bolt centerguide that would be interchangeable with the current production T156 unit for the M1 tank track. The unit was to be more durable and equal to or less than the weight of the T156 centerguide.			
20. DISTRIBUTION / AVAILABILITY OF ABSTRACT <input checked="" type="checkbox"/> UNCLASSIFIED/UNLIMITED <input type="checkbox"/> SAME AS RPT. <input type="checkbox"/> DTIC USERS		21. ABSTRACT SECURITY CLASSIFICATION Unclassified	
22a. NAME OF RESPONSIBLE INDIVIDUAL Joseph O. Fix		22b. TELEPHONE (Include Area Code) (313) 574-8681	22c. OFFICE SYMBOL AMSTA-RTT

THIS PAGE LEFT BLANK INTENTIONALLY

## TABLE OF CONTENTS

Section	Page
1.0. INTRODUCTION . . . . .	7
2.0. OBJECTIVE . . . . .	7
3.0. CONCLUSIONS . . . . .	7
4.0. RECOMMENDATIONS . . . . .	8
4.1. <u>Cap Construction</u> . . . . .	8
4.2. <u>Bolt Torque Requirement</u> . . . . .	8
4.3. <u>General</u> . . . . .	8
5.0. DISCUSSIONS . . . . .	8
5.1. <u>Background</u> . . . . .	9
5.2. <u>Materials</u> . . . . .	9
5.3. <u>Design</u> . . . . .	9
5.4. <u>Fabrication</u> . . . . .	14
5.5. <u>Testing</u> . . . . .	14
5.5.1. Lab Test . . . . .	14
5.5.2. Field Test . . . . .	15
SELECTED BIBLIOGRAPHY . . . . .	21
APPENDIX A. STRAIN GAGE STRESS CHARTS . . . . .	A-1
APPENDIX B. PHOTOELASTIC STRESS CHARTS AND PHOTOGRAPHS . . . . .	B-1
APPENDIX C. GENERAL REFERENCE INFORMATION . . . . .	C-1
DISTRIBUTION LIST . . . . .	Dist-1

THIS PAGE LEFT BLANK INTENTIONALLY

LIST OF ILLUSTRATIONS

Figure	Title	Page
5-1.	T156 Centerguide . . . . .	10
5-2.	T158 Centerguide . . . . .	10
5-3.	T156 vs. T158 Centerguide Wear Area Comparison . . .	11
5-4.	FMC Track Test Machine . . . . .	17
5-5.	T156 Centerguide Yield Indication . . . . .	19

LIST OF TABLES

Table	Title	Page
5-1.	T156 vs T158 Sectional Properties Comparison At High-Stressed Areas . . . . .	12

THIS PAGE LEFT BLANK INTENTIONALLY

## 1.0. INTRODUCTION

This final technical report is prepared by FMC Steel Products Division under contract number DAAE07-85-R-058 with the United States Army Tank-Automotive Command (TACOM). It describes the development and testing of a two-bolt centerguide assembly (designated XT158) proposed to replace the production single-bolt T156 unit. Two of the specific problems associated with the current unit are: 1) Due to the forked design with the bolt in the middle, the guide cannot be easily disassembled in service because the forks are sometimes bent inwards, thus making the nut inaccessible; 2) The T156 is prone to pin pull through due to the clamping bolt being between the two pins.

The T158 assembly solves both of these problems in addition to providing better track guidance and stability, higher design strength, and a more obscured natural frequency.

## 2.0. OBJECTIVE

The objective of this project was to design, develop, and manufacture a two-bolt domed centerguide assembly based on a concept supplied by TACOM Research, Development & Engineering (RD&E) Center. The assembly was to be compatible with the M1 track (both standard production T156 and development T158 designs), and as a target was to be equal to or less than the weight of the T156 centerguide.

## 3.0. CONCLUSIONS

The two-bolt centerguide developed under this contract has proven to be a good design. This design solves all of the problems associated with the production T156 unit plus it gives some added benefits. It fits the same envelope as the T156, it is stronger, more durable, and less prone to damaging roadwheels in the event of a track misguide. Field testing to date on a version for the FMC XT158S1.5 experimental track has shown no problems in more than 20,000 test miles. Limited testing on the first iteration for the 1.375-inch pin diameter (production T156) track took place in the summer of 1985, and it showed only minor problems. These problems were corrected in the final design and verified by lab test. The target of not exceeding the weight of the T156 unit was not achieved. The final two-bolt design is .6 pounds heavier, or 1.1 pounds heavier when using the optional machined cap. However, the benefits achieved in performance should compensate for the slight weight penalty. One benefit of particular interest is the lower natural frequency and amplitude which reduces the high-frequency track signature experienced with the

forked design.

#### 4.0. RECOMMENDATIONS

##### 4.1. Cap Construction

The centerguide cap should be of forged construction. Due to the time constraint, number of iterations required, and an attempt to keep development cost down, most of the caps supplied under this contract are of the optional machined design. However, field testing has been conducted on the forged cap design for the 1.5-inch pin diameter (XT158S1.5 track) configuration with excellent results. The 1.375-inch pin design cap will be stronger because the forgings for both designs are the same. The only difference is the amount of stock removed. This means that the 1.375-inch pin design forged cap will have slightly thicker sections.

##### 4.2. Bolt Torque Requirement

The bolts specified for the two-bolt assembly are 3/4-16 Unified Fine-thread (UNF) by 3.25 inches long, grade 8, per MS90727-192. The nut is a special capped 3/4-16UNF locking nut per military specification number MIL-N-45913. Both items are cadmium or zinc plated, and oil coated by the vendor. This means that the friction to tighten the assembly is substantially reduced and the torque required is not that of standard, uncoated, 3/4-inch, grade 8 bolts. Also, the design of the cap is such that it could yield if the bolts are torqued too tightly. This is crucial since the assembly is further preloaded due to track tensioning, and is subjected to severe fatigue service loads. It is for this reason that the assembly torque specified and recommended is only 210 to 225 foot-pound(ft-lb). This torque should also be applied in equal increments from one bolt to the other to ensure that stress distribution is maximized. Strain gage tests were conducted in which one bolt was tightened completely before the other one, and in both cases the cap yielded on the first-torqued-bolt side. These results are tabulated in Appendix A. Field testing to date has shown that there is no loosening or other problems associated with this low-torque approach.

##### 4.3. General

Due to the success achieved on this project it is recommended that the single-bolt T156 centerguide be replaced with the two-bolt T158 design.

#### 5.0. DISCUSSION

### 5.1. Background

The current production M1 track (T156) incorporates a single-bolt forked centerguide (see figure 5-1). This unit has consistently been a major cause of track work in the field due to the forks bending, the centerguide yielding and allowing the pins to pull through, or the unit failing due to fatigue cracks. The first problem negates the capability of replacing the two mating blocks without the aid of a cutting torch, and it compromises the proper guiding of the track. The second problem is even more severe because the track could separate while the vehicle is in motion. This is especially undesirable while on maneuver or negotiating a side slope. The TACOM-proposed two-bolt centerguide (see figure 5-2) eliminates all of these problems, and provides some additional benefits.

### 5.2. Materials

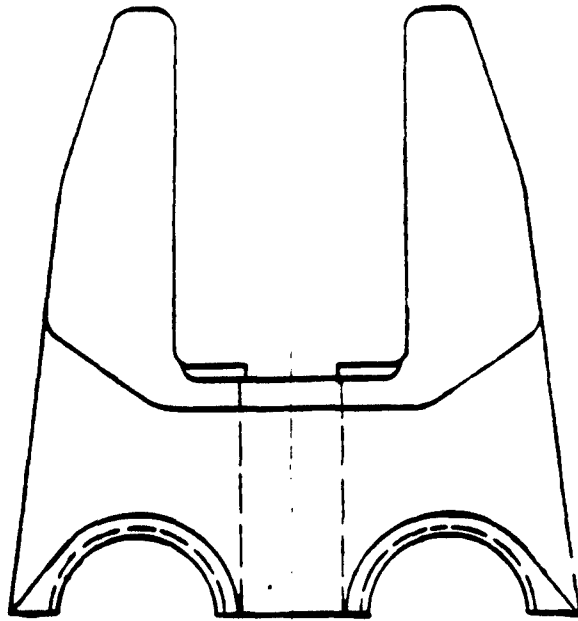
The material selected for the centerguide and cap was American Iron and Steel Institute (AISI) grade 4140 steel. This is the same material that is used on the production unit, and is more than adequate for the two-bolt design. AISI 4140 exhibits good hardening ability and fatigue life, and it has an excellent machinability rating which aids in keeping the unit cost down.

### 5.3. Design

The two-bolt centerguide was designed to the basic envelope of the production T156 unit for interchangeability. The pin hole centers remained the same so as not to change the track pitch, and the overall height also remained the same. Although the induction-hardened wear area geometry is different, the actual surface area is very similar (see figure 5-3).

The weakest area that has to resist side or lateral loading on the T156 centerguide is the base of the forks. Since the forks are not connected above the base, each one has to react independently depending on the position of the roadwheels. In the event of a track misguide, the forks have to react independently also to resist the off-track roadwheel loading. The T158 centerguide was designed with greater sectional properties than the T156 to resist these load conditions. The forked or ribbed sections are joined by a .25-inch web section, and they are also joined at the top. This integral design concept uses the material more efficiently to distribute stresses. The modulus of the section of the T158 which carries the same loads as the T156 forked base is 62.8 percent more in the x direction, and 944 percent more in the y direction. Table 5-1. shows the difference in sectional properties

(A) Front View



(B) Side View

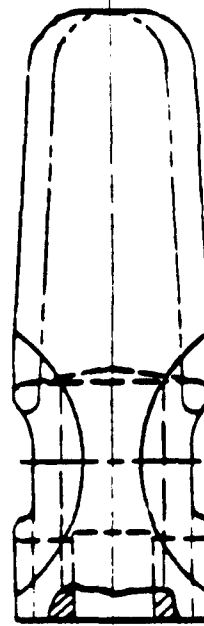
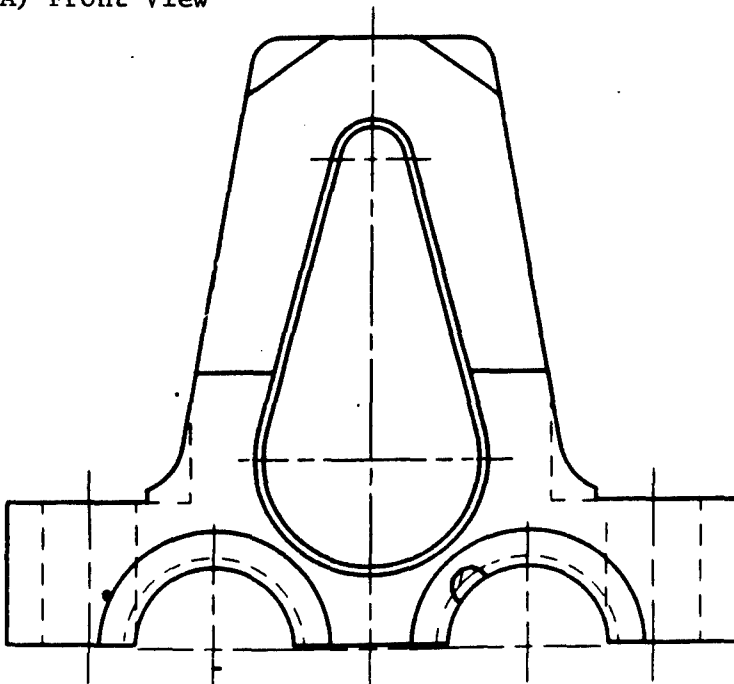


Figure 5-1. T156 Centerguide

(A) Front View



(B) Centerline  
Sectional  
View

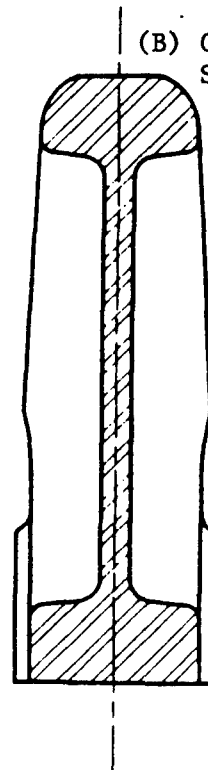
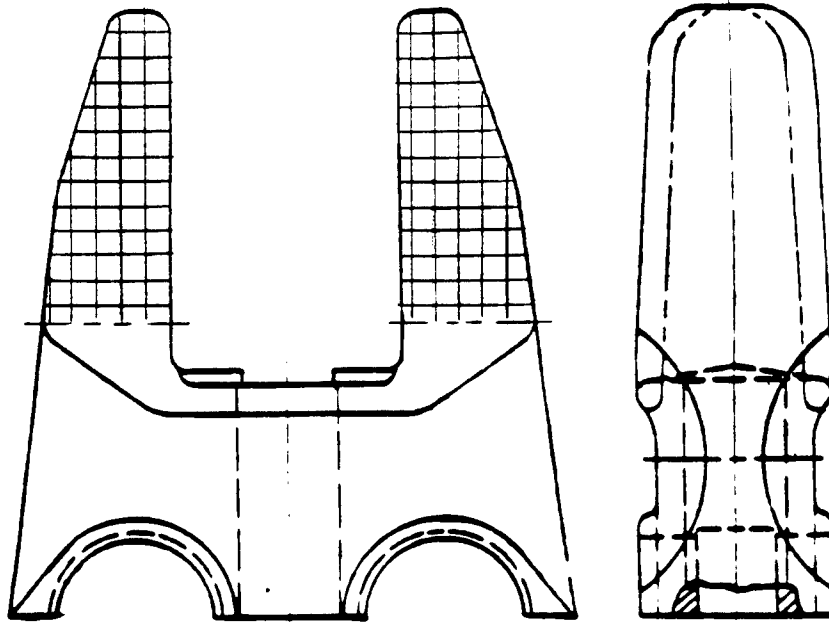


Figure 5-2. T158 Centerguide

T156 Centerguide



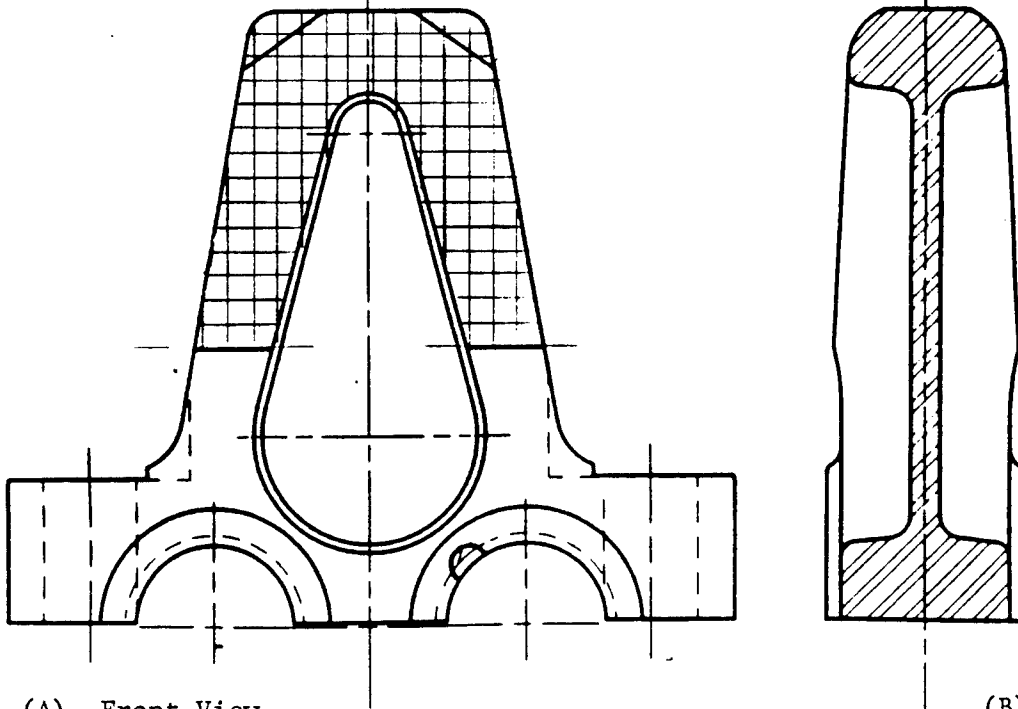
(A) Front View

(B) Side View



Centerguide Wear Area due to Roadwheel Guiding

T158 Centerguide



(A) Front View

(B) Centerline Sectional View

Figure 5-3. T156 vs. T158 Centerguide Wear Area Comparison

Sectional Properties:

	<u>T156</u>	<u>T158</u>
Moment of Inertia(I):	x .2520099 in. <sup>4</sup>	0.4004679 in. <sup>4</sup>
	y .1290280 in. <sup>4</sup>	3.2067960 in. <sup>4</sup>
Section Modulus(Z):	x .3036263 in. <sup>3</sup>	0.49440480 in. <sup>3</sup>
	y .1968943 in. <sup>3</sup>	2.05563800 in. <sup>3</sup>
Radius of Gyration(R):	x .4168242 in.	0.4106832 in.
	y .2982539 in.	1.162141 in.

Table 5-1. T156 vs T158 Sectional Properties Comparison at High-Stressed Areas

at the point in question for both centerguides, and the following calculations illustrate the corresponding difference in stresses for both units:

Sample Stress Calculations

Load: x-direction 3,000 pounds at 3.18-inch moment arm  
 y-direction 10,000 pounds at 3.18-inch moment arm

$$\text{stress}(S) = \text{load}(P) \times \text{moment arm}(L) / \text{section modulus}(Z)$$

$$= \text{pounds/square inch}(\text{psi})$$

Therefore:

<u>T156</u>	<u>T158</u>
$S_x = \frac{3,000 \times 3.18}{.3036263} = 31,400 \text{ psi}$	$\frac{3,000 \times 3.18}{.4944048} = 19,296 \text{ psi}$
$S_y = \frac{10,000 \times 3.18}{.1968943} = 161,508 \text{ psi}$	$\frac{10,000 \times 3.18}{2.055638} = 15,470 \text{ psi}$

With the incorporation of two bolts on the outside of the pins instead of one on the inside, the lateral envelope section increased considerably. This posed an interference problem with the bolt caps as the guide goes around the sprockets. For this reason, the final design resulted in the bolt flange areas being smaller than was originally selected, but adequate. This area turned out to be the weakest section, but will be increased by .125 inches when the lock washers are eliminated. Field tests on the version for the 1.5-inch pin (XT158S1.5) track with no washers, and the 1.375-inch pin track with flat washers showed that lock washers are not required when the special locking nuts are used.

The major advantages of the two-bolt T158 concept is that the material section that has to resist off-track roadwheel loading is increased by magnitudes over the T156, and the outside bolting arrangement acts as a fail-safe measure. The other advantage is that in the event of a track misguide there is less damage to the roadwheels and centerguides.

Two cap designs were considered. The design machined from alloy bar was adapted for testing due to the time constraint. The forged cap design shows more evenly distributed stresses, it weighs .5 pounds less, and it is more cost-effective than

the completely machined version. A situation exists in both cap designs that is unique. The grade 8, 3/4-16UNF bolts specified will cause the cap to yield slightly when torqued to their maximum allowable torque. When the track is under load it imparts additional clamp forces to the bolt via the center-guide and cap. These forces alleviate the stresses on the cap somewhat, but increase the bolt load. For this reason the torque specified on the two-bolt assembly is only 210 to 225 ft-lb. Field testing to date has shown that this approach is satisfactory. Even if the bolts are torqued to their maximum the effect on the cap is only strain hardening, but the bolts will see higher clamp loading than they were designed for and removal of the centerguide assembly will be complicated because of the cap geometry change(Also see section 4.2).

The nuts specified on the two-bolt assembly are special locking nuts with protective caps electrically welded on. This has proven to be an aid in disassembly after service use because without the protective cap the exposed bolt threads are easily damaged, causing the nuts to be difficult to remove.

#### 5.4. Fabrication

The centerguide is forged from billet stock, heat treated, and then machined. After machining the unit is induction hardened in the area where the roadwheels are guided. The forged cap is made in the same fashion except that there is no induction hardening requirement. The optional cap design is machined completely from bar stock. The bolts, nuts and lock washers are vendor-purchased items.

#### 5.5. Testing

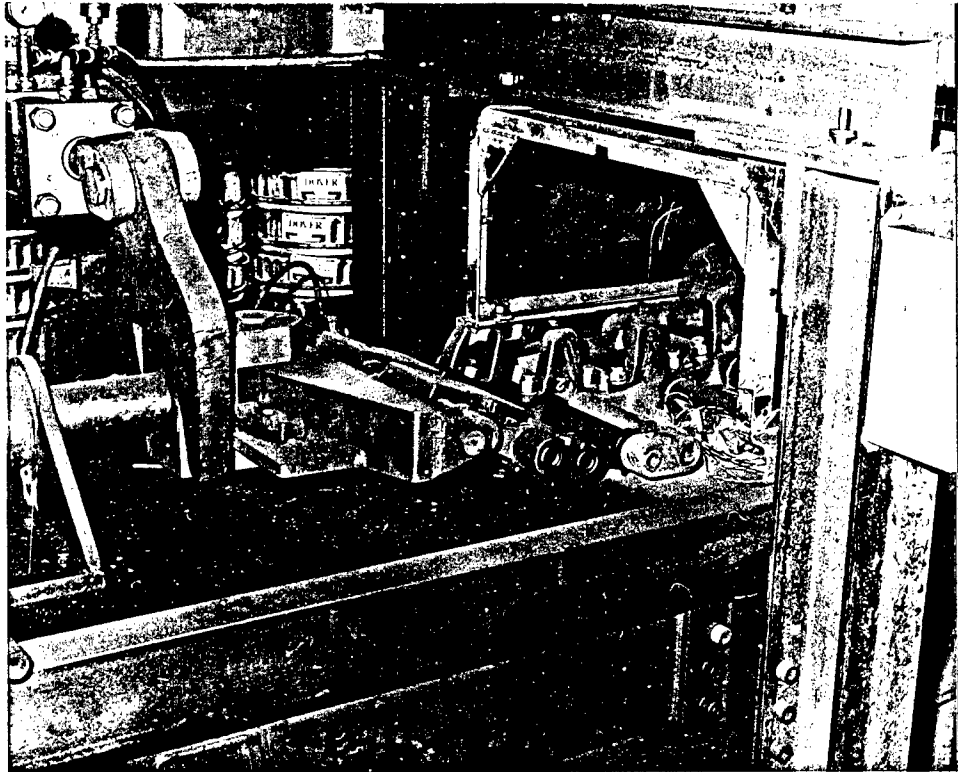
5.5.1. Lab Test. Both the centerguide and caps were photoelastically stress analyzed using the PhotoStress method. The high-stressed areas were identified from this analysis, then strain gages were applied to an identical specimen. The types of strain gages used were 45-degree rosettes. These types of gages were chosen so that the principle stress direction obtained from the photoelastic analysis could be verified. Although the contract scope included brittlecoat analysis, it was determined that this was not necessary due to the advanced photoelastic equipment used. We were able to determine principle stress direction and magnitude of the difference in  $\sigma_x$  and  $\sigma_y$  consistently. The findings were further backed up using the strain gage rosettes mentioned earlier rather than the conventional unigages which require that the direction already be known. See Appendices A through C for complete data and photographs.

The T156 production unit was run first to establish a baseline. The centerguide was assembled onto a five-shoe strip of

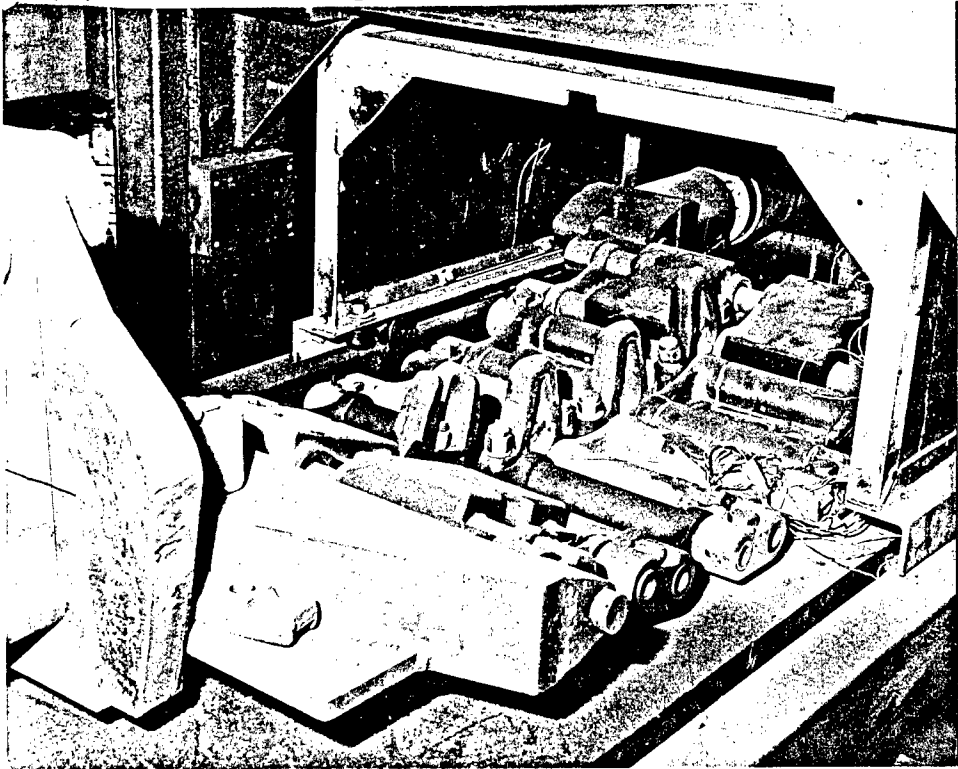
experimental T158 track and placed in a special FMC track test machine (see figure 5-4). The load conditions applied were: 60,000-lb tension only; 60,000-lb tension with 6,000-lb side load; 100,000-lb tension only; and 100,000-lb tension with 6,000-lb side load. The T156 unit yielded during the 100,000-lb tension test. The yielding occurred at the pin outer clamp area (see figure 5-5). The T158 assembly showed no signs of yielding in any area during testing, not even the initial prototype. The average stresses in the final two-bolt design were slightly higher than the prototype, but were more evenly distributed. The final design is also 1.6 pounds lighter.

5.5.2. Field Test. Field testing on the final T158 center-guide in the 1 3/8-inch configuration has been limited to a short RD&E run at Yuma Proving Grounds (YPG) in Arizona in March of 1986. There were no problems reported, but the test plan called for only 500 miles. Extensive testing was conducted on the earlier prototype version at YPG, Aberdeen, Maryland (APG) and Fort Hood, Texas in the summer of 1985. Three failures were reported at APG where the guide broke in the bolt flange area. Changes were incorporated into the final 1 3/8-inch and 1 1/2-inch designs to alleviate this problem. Testing to date on the 1 1/2-inch design has not produced a failure in over 20,000 cumulative test miles on a total of six test vehicles. One track achieved over 2,400 test miles without a centerguide failure. The 1 3/8-inch version will have similar results since the sectional area is approximately the same.

THIS PAGE LEFT BLANK INTENTIONALLY



(A) View Showing Pull Yoke and Twist Cylinder



(B) Close-Up View of A

Figure 5-4. FMC Track Test Machine

THIS PAGE LEFT BLANK INTENTIONALLY

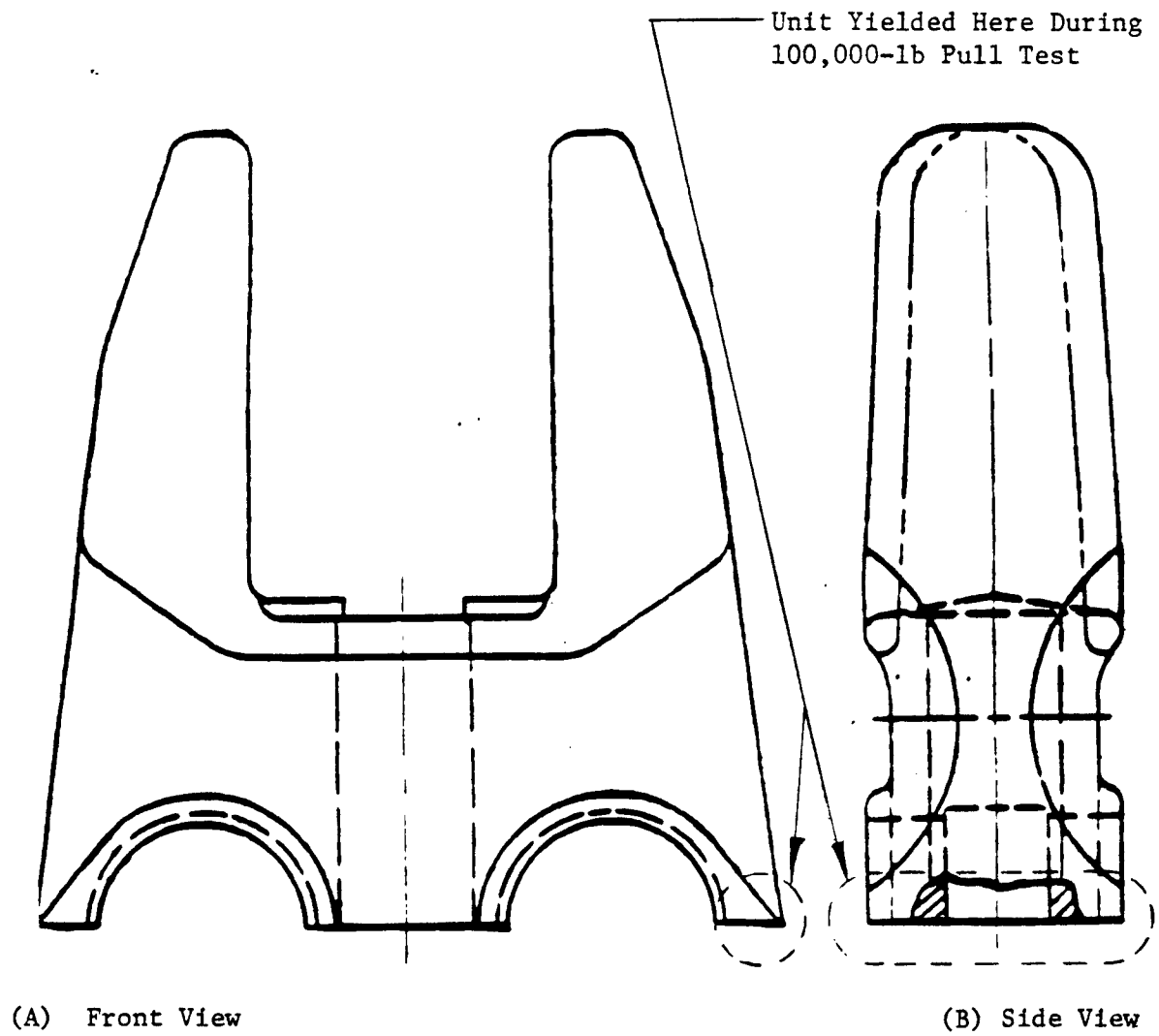


Figure 5-5. T156 Centerguide Yield Indication

**THIS PAGE LEFT BLANK INTENTIONALLY**

## SELECTED BIBLIOGRAPHY

- Boblenz, James N., "RD&E Center Technical Report Writing Style Manual," U. S. Army Tank-Automotive Command, Warren, MI (1986)
- Chandler, Harry E., "Technical Writer's Handbook," American Society For Metals," Metals Park, OH (1983)
- Errors Due To Transverse Sensitivity In Strain Gages, TN-509, Measurement Group Inc., Raleigh, N. C. (1982)
- Perry, C. C., "The Care And Feeding Of Strain Gage Rosettes," Measurement Group, Raleigh, N. C. (1979)
- Zandman, Felix, "Photoelastic Coatings," Society For Experimental Stress Analysis, Westport, CT (1977)

THIS PAGE LEFT BLANK INTENTIONALLY

**APPENDIX A**

**STRAIN GAGE STRESS CHARTS**

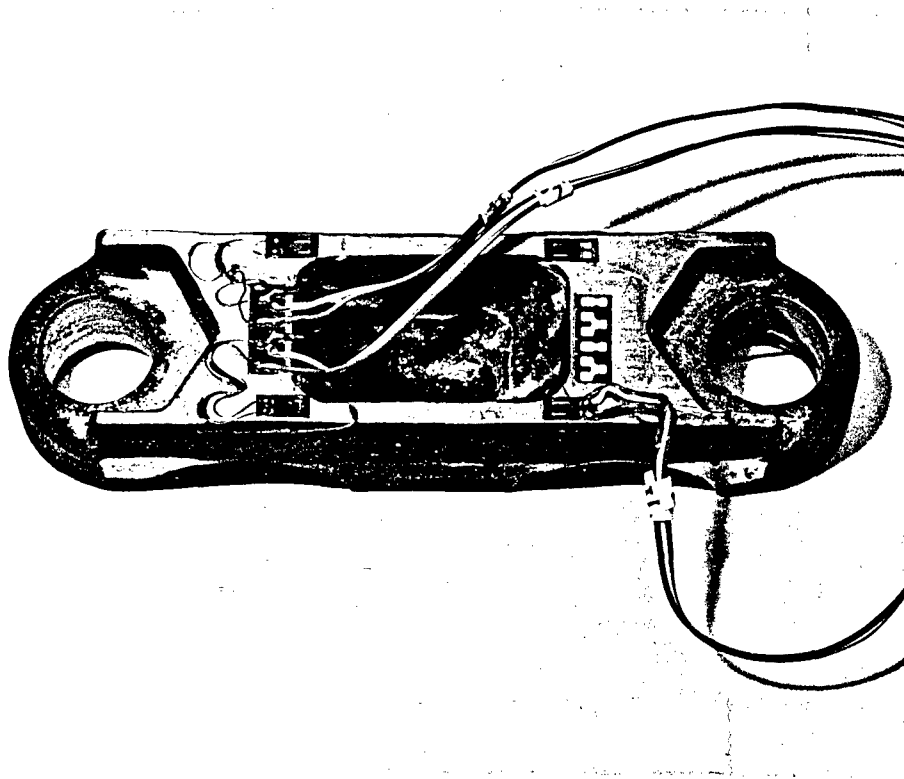
**XT158 Centerguide Cap Strain Gage Readings  
(Final)**

<b>Gage Number</b>	<b>Assembly Strain (.000010 in/in)</b>	<b>Assembly Stress (psi)</b>
1	2,329	69,870
2	2,339	70,170
3	2,358	70,740

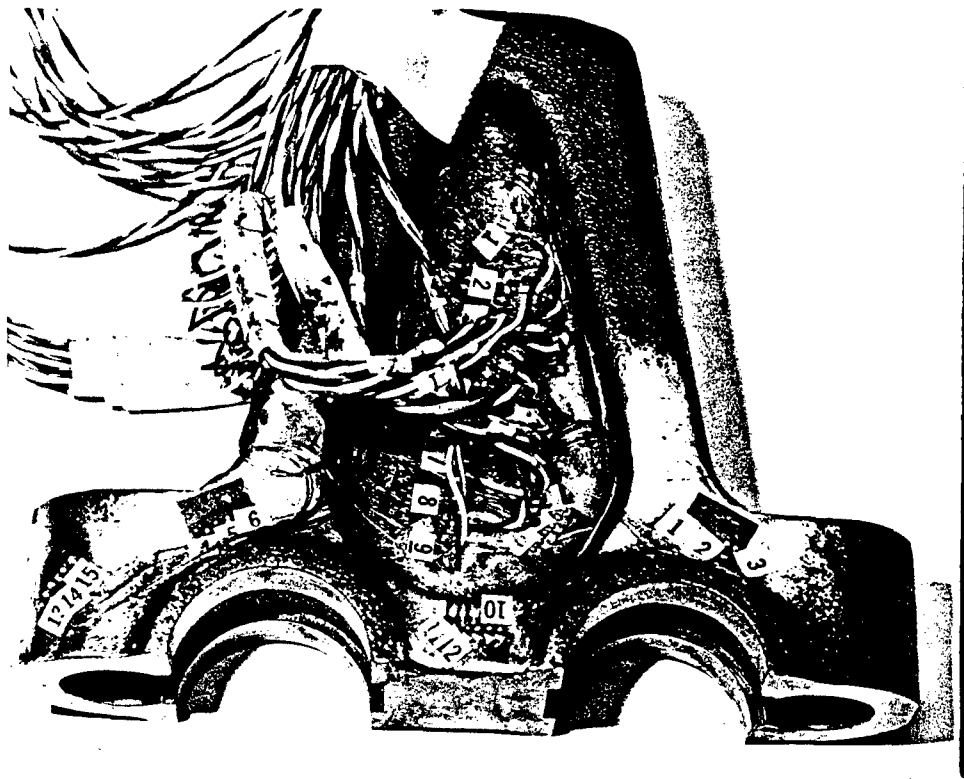
**Example Calculation:**

$$\begin{aligned}\text{Stress} &= \text{Strain} \times \text{Young's Modulus} \\ &= .002329 \text{ in/in} \times 30,000,000 \text{ psi} \\ &= 69,870 \text{ psi}\end{aligned}$$

**Note: Due to the uniaxial stress field in the cap,  
simple unigages were used.**



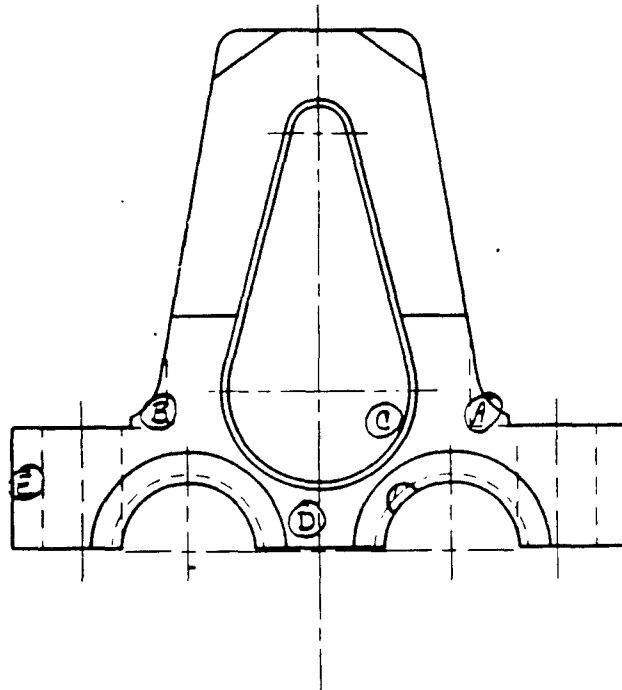
T-158 Centerguide Cap Strain Gage Placement



T-158 Centerguide Strain Gage Placement

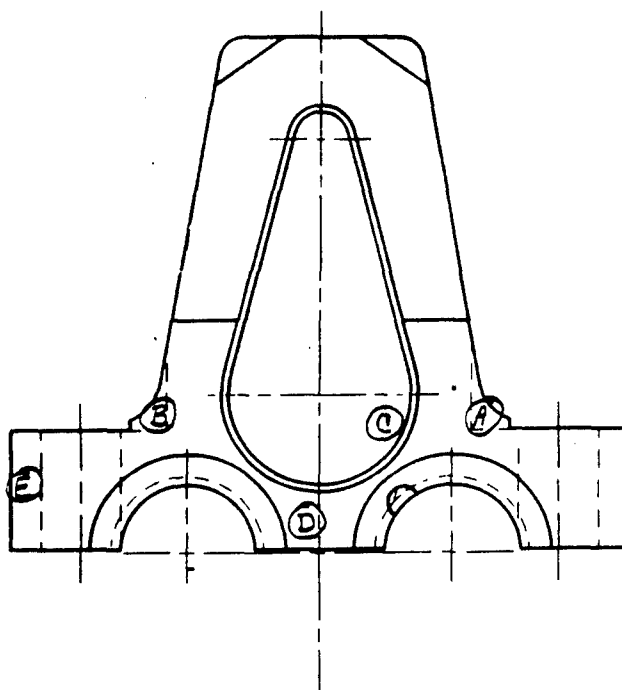
27 NOVEMBER 1985  
 XT1 CENTERGUIDE  
 ASSEMBLY STRESS (WITH GAGES FACING CYLINDER)

Point	Max Strain (u IN/IN)	Min Strain ( u IN/IN)	Max Stress (PSI)	Min Stress (PSI)	Prin. Angle (DEGREES)
A	2984.095	298.3617	100577.1	38118.21	36.45544
B	2456.611	650.3346	86642.9	44636.47	-32.32942
C	822.5	-1112.39	16374.29	-28623.15	1.178376
D	76.00325	-225.8781	343.8785	-6676.618	-31.92461
E	688.2496	-532.4586	17485.64	-10902.93	37.97528



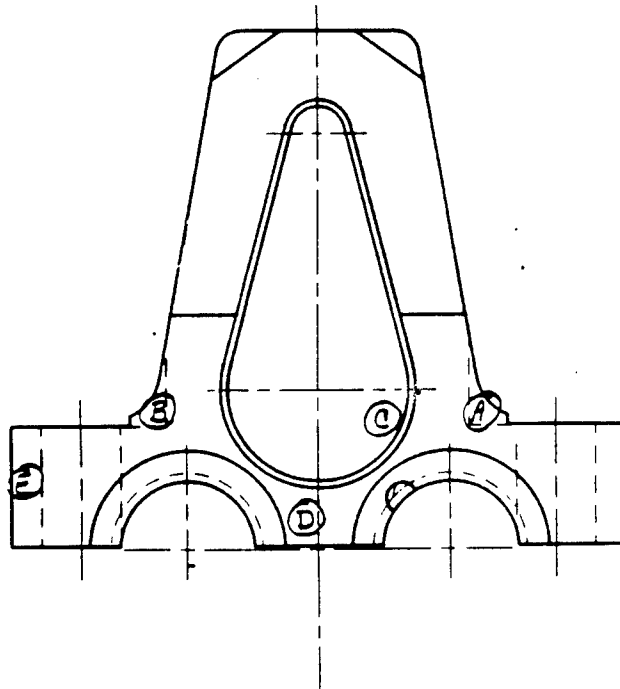
27 NOVEMBER 1985  
 XT1 CENTERGUIDE  
 ASSEMBLY STRESS

Point	Max Strain (u IN/IN)	Min Strain ( u IN/IN)	Max Stress (PSI)	Min Stress (PSI)	Prin. Angle (DEGREES)
A	2624.393	223.2294	88081.53	32240.52	35.41824
B	2332.287	1081.31	86664.47	57572	22.35583
C	862.0786	-950.8202	19205.4	-22955.05	22.40521
D	106.4866	-213.9626	1455.533	-5996.774	-21.16931
E	826.6715	-814.8393	19337.31	-18837.36	37.60016



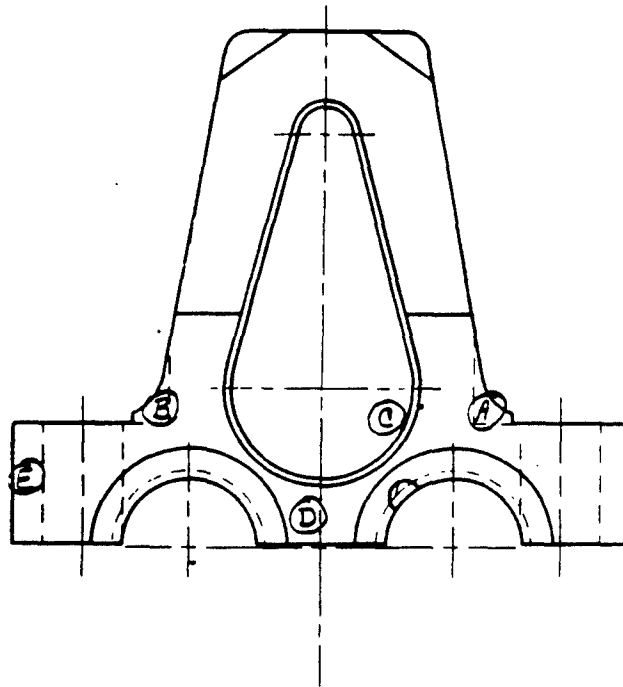
27 NOVEMBER 1985  
 YTI CENTERGUIDE  
 50000 LB. TENSION

Point	Max Strain ( $\mu$ IN/IN)	Min Strain ( $\mu$ IN/IN)	Max Stress (PSI)	Min Stress (PSI)	Prin. Angle (DEGREES)
A	2665.84	168.964	88923.66	30856.78	41.3239
B	2988.263	611.6916	103689.9	48420.82	-35.84153
C	1294.504	-780.7883	34984.46	-13278.16	-15.76377
D	64.26296	-84.96934	1297.8	-2172.719	-12.12069
E	842.4941	-855.3124	19471.13	-20012.74	37.02277



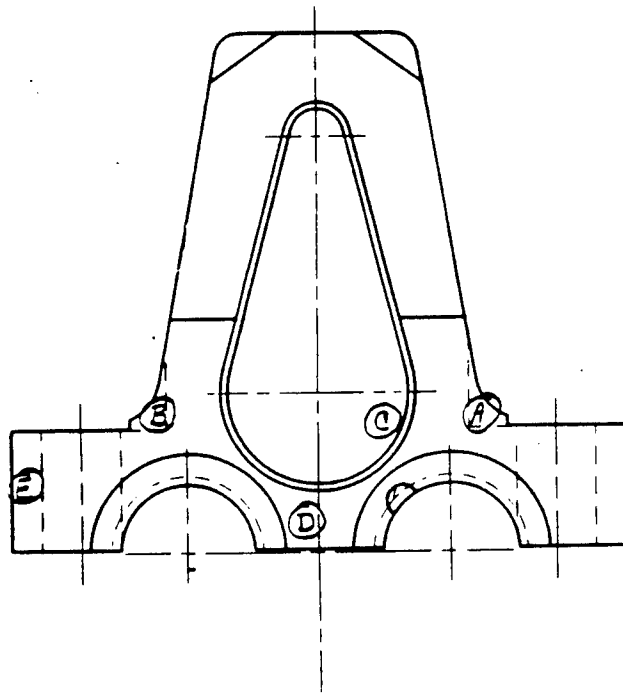
27 NOVEMBER 1985  
 XT1 CENTERGUIDE  
 60000 LB. TENSION AND 10682 LB. SIDE LOAD (WITH GAGES FACING CYLINDER)

Point	Max Strain (u IN/IN)	Min Strain ( u IN/IN)	Max Stress (PSI)	Min Stress (PSI)	Prin. Angle (DEGREES)
A	3195.202	293.3327	107444.1	39958.76	37.96397
C	2579.307	667.6528	90826.27	46369.2	-32.64193
C	1322.105	-978.9702	34006.01	-19507.37	-7.359645
D	63.52716	-197.6257	203.5934	-5869.73	-34.83685
E	745.398	-627.0757	18458.76	-13459.23	36.98513



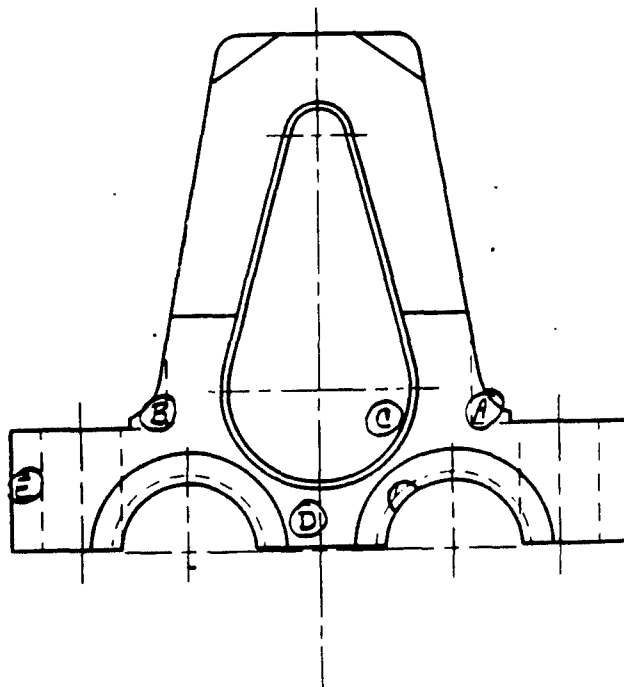
27 NOVEMBER 1985  
 XT1 CENTERGUIDE  
 60000 LB. TENSION AND 12000 LB. SIDE LOAD (WITH GAGES FACING CYLINDER)

Point	Max Strain (u IN/IN)	Min Strain ( u IN/IN)	Max Stress (PSI)	Min Stress (PSI)	Prin.Angle (DEGREES)
A	3206.42	309.7236	107967.2	40602.2	37.14651
B	2596.502	669.1922	91404.12	46582.96	-31.63566
C	1302.144	-958.0237	33551.18	-19010.87	-7.245531
D	-26.17714	-117.7816	-1976.213	-4106.55	-9.432336
E	746.6274	-630.2772	18468.62	-13552.42	36.96797



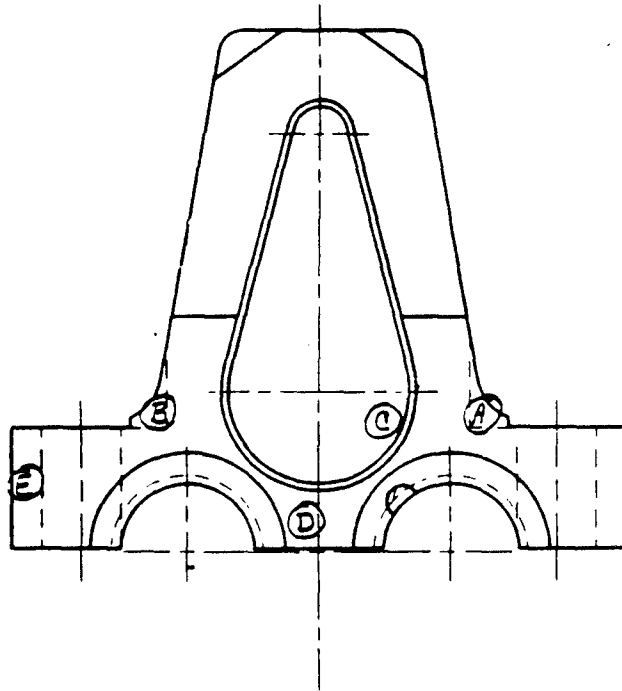
27 NOVEMBER 1985  
 XT1 CENTERGUIDE  
 60000 LB. TENSION AND 10682 LB. SIDE LOAD

Point	Max Strain (u IN/IN)	Min Strain ( u IN/IN)	Max Stress (PSI)	Min Stress (PSI)	Prin.Angle DEGREES
A	2605.617	22.1228	85556.27	25475	-42.50438
B	2937.783	569.4861	101635.6	46558.89	-41.5411
C	1385.564	-850.1555	37308.18	-14685.3	-14.57911
D	94.57662	-26.54133	2845.714	29.01684	24.4474
E	864.3023	-870.2184	20043.86	-20293.83	37.38594



27 NOVEMBER 1985  
 XT1 CENTERGUIDE  
 50000 LB. TENSION AND 50000 IN.-LB. TORSION

Point	Max Strain (u IN/IN)	Min Strain ( u IN/IN)	Max Stress (PSI)	Min Stress (PSI)	Prin. Angle (DEGREES)
A	2668.802	155.1558	88889.52	30432.63	41.96159
B	2930.562	618.1194	101861	48083.28	-36.4446
C	1298.518	-767.0538	35246.39	-12790.16	-15.48837
D	51.3022	-65.10645	1061.95	-1645.228	-11.69481
E	843.3156	-857.1198	19480.87	-20064.14	37.05308



12/10/85  
 XT158 (FINAL) CENTERGUIDE  
 UNEQUAL ASSEMBLY STRESS (SIDE A TORQUED FIRST)

Point	Max Strain (u IN/IN)	Min Strain ( u IN/IN)	Max Stress (PSI)	Min Stress (PSI)	Prin.Angle (DEGREES)
A	3976.452	391.6111	133484.1	49791.29	34.2282
B	1876.333	282.0618	63891.18	26670.84	-19.62075
C	1476.412	-1896.456	30559.88	-48184.11	4.664408
D	215.6786	-587.4077	1576.037	-17173.06	31.04281
E	297.217	-248.902	7388.53	-5361.33	37.56735

12/10/85  
 XT158 (FINAL) CENTERGUIDE  
 RESIDUAL ASSEMBLY STRESS AT A

Point	Max Strain (u IN/IN)	Min Strain ( u IN/IN)	Max Stress (PSI)	Min Stress (PSI)	Prin.Angle (DEGREES)
A	45.17921	1.163675	1486.028	458.4283	22.38671

12/10/85  
 XT158 (FINAL) CENTERGUIDE  
 UNEQUAL ASSEMBLY STRESS (SIDE B TORQUED FIRST)

Point	Max Strain (u IN/IN)	Min Strain ( u IN/IN)	Max Stress (PSI)	Min Stress (PSI)	Prin.Angle (DEGREES)
-----	-----	-----	-----	-----	-----
A	2285.756	201.969	76514.41	27865.68	27.41162
B	3309.664	1022.902	117586.7	64199.28	-28.28316
C	580.6233	-752.1905	11958.82	-19157.45	-23.31594
D	217.5623	-560.6968	1886.11	-16283.36	-28.34604
E	904.8994	-793.4793	22162.92	-17487.95	36.60022

12/10/85  
 XT158 (FINAL) CENTERGUIDE  
 RESIDUAL ASSEMBLY STRESS AT B

Point	Max Strain (u IN/IN)	Min Strain ( u IN/IN)	Max Stress (PSI)	Min Stress (PSI)	Prin.Angle (DEGREES)
-----	-----	-----	-----	-----	-----
B	123.8343	-86.36556	3239.751	-1667.637	-34.90132

**THIS PAGE LEFT BLANK INTENTIONALLY**

APPENDIX B

PHOTOELASTIC STRESS CHARTS AND PHOTOGRAPHS

PHOTOELASTIC STRESS ANALYSIS - XT1 PROJECT  
 DATA POINT STRESS CALCULATIONS  
 TEST SPECIMEN: T-156 CENTERGUIDE

SEPT, 84

TEST MODE: 60,000 lb. (TENSION)

\*\*\*\*\*

POINT	SHEET	N	t	K VALUE	(s1-s2)/N	s1-s2
1	1	3.74	.091	.081	35810	133928
2	1	2.67	.106	.081	30742	82082
3	1	3.84	.113	.081	28838	110738
4	1	3.93	.113	.081	28838	113333
5	1	2.89	.113	.081	28838	83342
6	1	3.99	.093	.081	35040	139808
7	1	1.3	.106	.081	30742	39965
8	1	2.29	.106	.081	30742	70400

TEST MODE: 100,000 lb. (TENSION)

\*\*\*\*\*

POINT	SHEET	N	t	K VALUE	(s1-s2)/N	s1-s2
1	1	7.14	.091	.081	35810	255681
2	1	4	.106	.081	30742	122969
3	1	3.46	.113	.081	28838	99779
4	1	4.44	.113	.081	28838	128040
5	1	3.84	.113	.081	28838	110738
6	1	7.14	.093	.081	35040	250183
7	1	1.61	.106	.081	30742	49495
8	1	3.35	.106	.081	30742	102987

TEST MODE: 100,000 lb. (TENSION)

6,000 lb. (SIDE LOAD)

\*\*\*\*\*

POINT	SHEET	N	t	K VALUE	(s1-s2)/N	s1-s2
1	1	7.14	.091	.081	35810	255681
2	1	3.76	.106	.081	30742	115591
3	1	4.94	.113	.081	28838	142459
4	1	-----	.113	.081	28838	0
5	1	4.17	.113	.081	28838	120254
6	1	7.13	.093	.081	35040	249833
7	1	1.6	.106	.081	30742	49188
8	1	4.45	.106	.081	30742	136803

PHOTOELASTIC STRESS ANALYSIS - XT1 PROJECT  
 DATA POINT STRESS CALCULATIONS  
 TEST SPECIMEN: XT1 CENTERGUIDE (SOLID PROTOTYPE)  
 5/16/85

TEST MODE: 60,000 lb. (TENSION)

\*\*\*\*\*

POINT	SHEET	N	t	K VALUE	(s1-s2)/N	s1-s2
1	1	1.92	.108	.074	33027	63412
2	1	2.34	.108	.074	33027	77284
3	1	1.17	.114	.074	31289	36608
4	1	.93	.098	.074	36397	33850
5	1	.8	.105	.074	33971	27177

TEST MODE: 60,000 lb. (TENSION)  
 6,000 lb. (SIDE LOAD)

\*\*\*\*\*

POINT	SHEET	N	t	K VALUE	(s1-s2)/N	s1-s2
1	1	2.8	.108	.074	33027	92476
2	1	3.15	.108	.074	33027	104036
3	1	2.32	.114	.074	31289	72590
4	1	1.15	.098	.074	36397	41857
5	1	1.18	.105	.074	33971	40086

TEST MODE: 97,300 lb. (TENSION)

\*\*\*\*\*

POINT	SHEET	N	t	K VALUE	(s1-s2)/N	s1-s2
1	1	.78	.108	.074	33027	25761
2	1	1.98	.018	.074	198163	392363
3	1	1.94	.114	.074	31289	60701
4	1	1.61	.098	.074	36397	58600
5	1	1.17	.105	.074	33971	39746

TEST MODE: ASSEMBLY STRESS (NO LOAD)

\*\*\*\*\*

POINT	SHEET	N	t	K VALUE	(s1-s2)/N	s1-s2
1	1	1	.108	.074	33027	33027
2	1	2.04	.108	.074	33027	67376
3	1	1.16	.114	.074	31289	36295

PHOTOELASTIC STRESS ANALYSIS - XT1 PROJECT  
 DATA POINT STRESS CALCULATIONS  
 TEST SPECIMEN: XT1 CENTERGUIDE (PROTOTYPE)

DATE: NOV, 84

TEST MODE: 60,000 lb. (TENSION)

\*\*\*\*\*

POINT	SHEET	N	t	K VALUE	(s1-s2)/N	s1-s2
1	1	1.15	.111	.0825	28824	33147
2	1	1.35	.088	.0825	36357	49082
3	1	1.26	.096	.0825	33327	41993
4	1	1.08	.086	.0825	37203	40179
5	1	---	.104	.0825	30764	0

TEST MODE: 60,000 lb. (TENSION)  
 6,000 lb. (SIDE LOAD)

\*\*\*\*\*

POINT	SHEET	N	t	K VALUE	(s1-s2)/N	s1-s2
1	1	1	.111	.0825	28824	28824
2	1	1.78	.088	.0825	36357	64716
3	1	1.71	.096	.0825	33327	56990
4	1	1.37	.086	.0825	37203	50968
5	1	---	.104	.0825	30764	0

TEST MODE: 100,000 lb. (TENSION)

\*\*\*\*\*

POINT	SHEET	N	t	K VALUE	(s1-s2)/N	s1-s2
1	1	.78	.111	.0825	28824	22483
2	1	1.98	.088	.0825	36357	71987
3	1	1.94	.096	.0825	33327	64655
4	1	1.61	.086	.0825	37203	59896
5	1	1.17	.104	.0825	30764	35994

TEST MODE: 100,000 lb. (TENSION)  
 6,000 lb. (SIDE LOAD)

\*\*\*\*\*

POINT	SHEET	N	t	K VALUE	(s1-s2)/N	s1-s2
1	1	.79	.111	.0825	28824	22771
2	1	2.39	.088	.0825	36357	86894
3	1	2.22	.096	.0825	33327	73987
4	1	1.88	.086	.0825	37203	69941
5	1	1.2	.104	.0825	30764	36917

PHOTOELASTIC STRESS ANALYSIS - XT1 PROJECT  
 DATA POINT STRESS CALCULATIONS  
 TEST SPECIMEN: XT1 C. G. STD TEARDROP (FORGED)  
 DATE: SEPT 17, 1985

TEST MODE: 60,000 lb. (TENSION)

\*\*\*\*\*

POINT	SHEET	N	t	K VALUE	(s1-s2)/N	s1-s2
A	1	3.02	.101	.11	23758	71750
C	1	1.38	.084	.11	28566	39422
D	1	1.76	.092	.11	26082	45905
E	1	3.1	.101	.11	23758	73650
F	1	2.42	.101	.11	23758	57495
G	1	2.59	.104	.11	23073	59759
H	1	1.17	.087	.11	27581	32270

TEST MODE: 60,000 lb. (TENSION)  
 6,000 lb. (SIDE LOAD)

\*\*\*\*\*

POINT	SHEET	N	t	K VALUE	(s1-s2)/N	0
A	1	3.45	.101	.11	23758	81966
C	1	2.13	.084	.11	28566	60846
D	1	1.86	.092	.11	26082	48513
E	1	3.42	.101	.11	23758	81253
F	1	2.78	.101	.11	23758	66048
G	1	3.11	.104	.11	23073	71757
H	1	1.51	.087	.11	27581	41648

TEST MODE: 100,000 lb. (TENSION)

\*\*\*\*\*

POINT	SHEET	N	t	K VALUE	(s1-s2)/N	s1-s2
A	1	3.06	.101	.11	23758	72700
C	1	1.43	.084	.11	28566	40850
D	1	1.78	.092	.11	26082	46427
E	1	3.28	.101	.11	23758	77927
F	1	2.78	.101	.11	23758	66048
G	1	2.54	.104	.11	23073	58605
H	1	1.73	.087	.11	27581	47716

TEST MODE: 100,000 lb. (TENSION)  
 6,000 lb. (SIDE LOAD)

\*\*\*\*\*

POINT	SHEET	N	t	K VALUE	(s1-s2)/N	s1-s2
A	1	3.5	.101	.11	23758	83154
C	1	2.19	.084	.11	28566	62560
D	1	1.82	.092	.11	26082	47470
E	1	3.56	.101	.11	23758	84579
F	1	3.14	.101	.11	23758	74601
G	1	3.25	.104	.11	23073	74987
H	1	1.98	.087	.11	27581	54611

TEST MODE: ASSEMBLY STRESS (NO LOAD)

\*\*\*\*\*

POINT	SHEET	N	t	K VALUE	(s1-s2)/N	s1-s2
A	1	3.61	.101	.11	23758	85767
C	1	1.84	.084	.11	28566	52562
D	1	1.44	.092	.11	26082	37559
E	1	3.17	.101	.11	23758	75313
F	1	2.32	.101	.11	23758	55119
G	1	2.56	.104	.11	23073	59067

## Explanation Of Photoelastic Stress Analysis Charts

### Legend:

- Point- The actual stress location measured
- Sheet- The photoelastic coating number assigned. Each sheet will exhibit slightly different physical characteristics that will vary stress readings
- N- The number of color fringes measured
- t- The thickness measured as close to the actual stress point as possible
- k- The fringe value of the sheet obtained by calibration
- s1-s2- This is the difference in principle stress as calculated from the formula below
- E- Young's Modulus of test part
- L- Wavelength of yellow light
- v- Poisson's ratio of test part

### Basic photoelastic stress formula:

$$s1-s2 = \frac{N \times E}{(1 + v)} \times \frac{L}{(2 \times t \times k)}$$

NOTE: s1-s2 was not separated in this analysis since it was felt that the accuracy to do this was not good enough, especially since the procedure was to be repeated with more accurate strain gages.

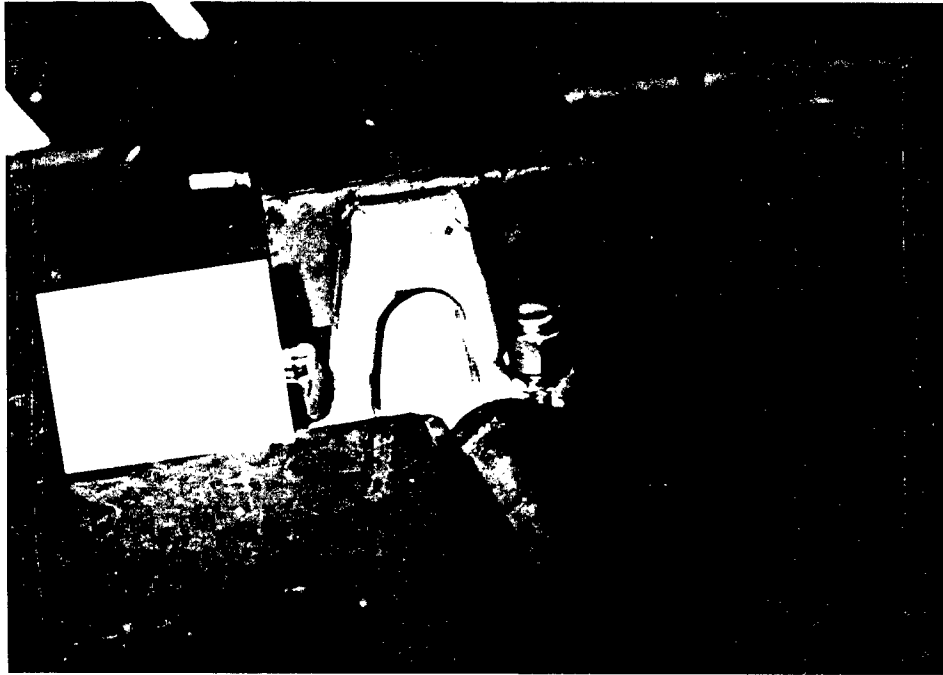
See additional information on photoelastic interpretation in appendix C.



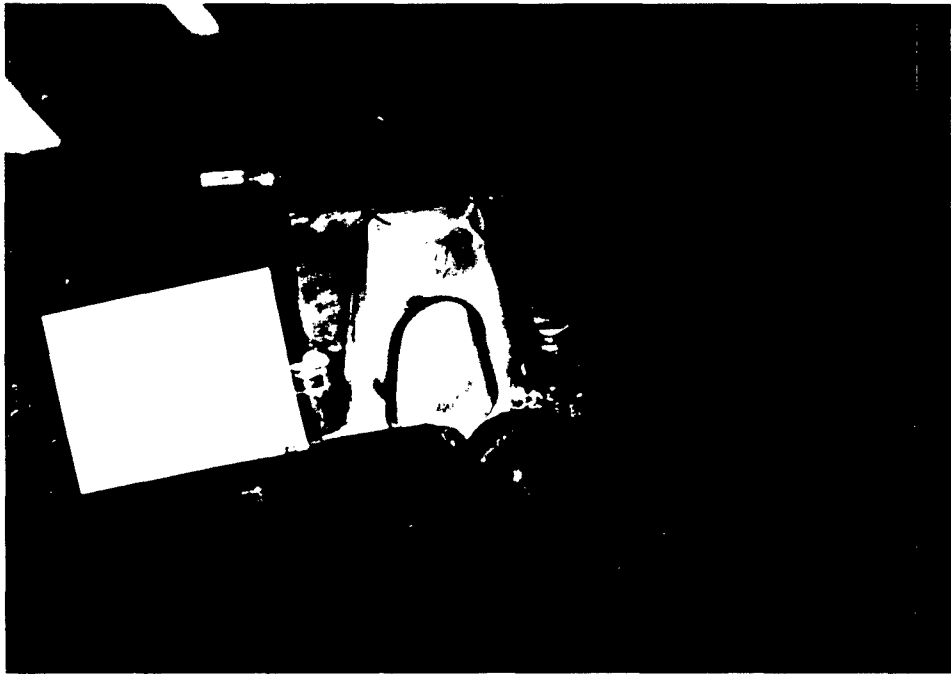
T-156 Centerguide Stress Distribution at 100,000  
lb Tensile Load



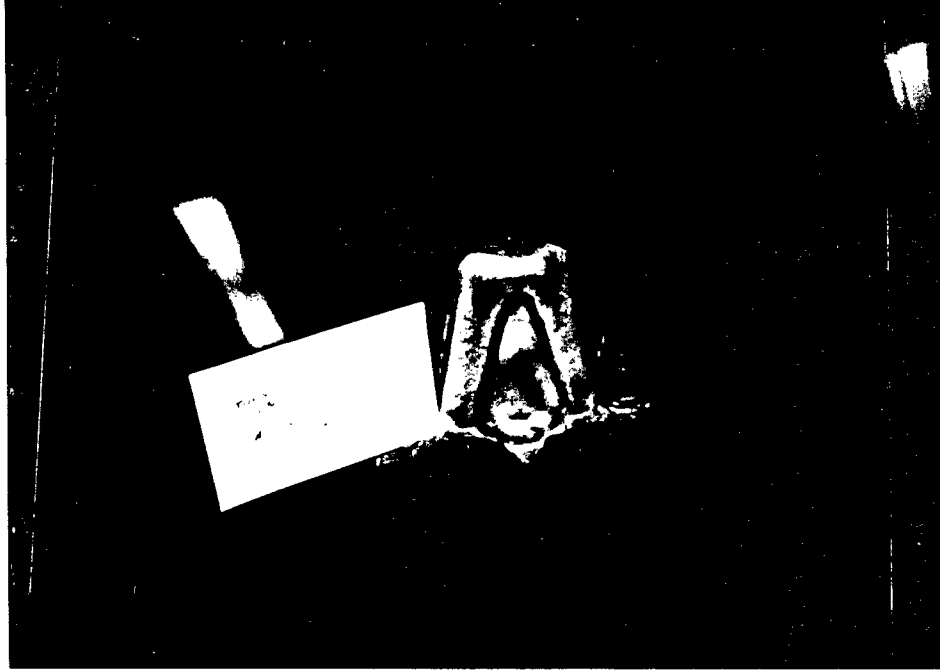
T-156 Centerguide Stress Distribution at 100,000  
Tensile and 6,000 lb Side Load



T-158 Prototype Stress Distribution at 60,000  
lb Tensile Load



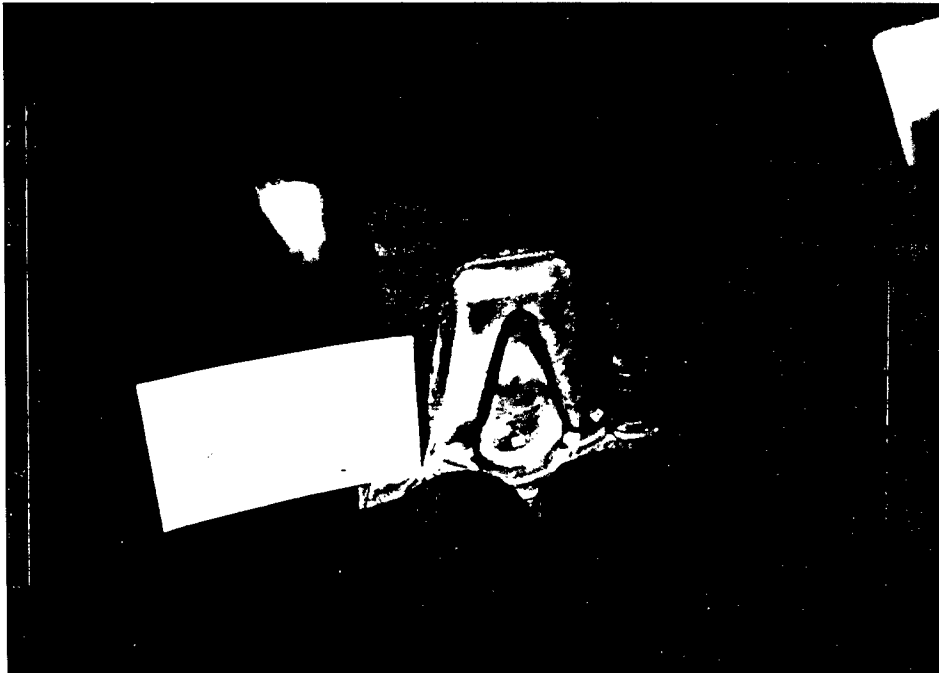
T-158 Prototype Stress Distribution at 60,000  
lb Tensile and 6,000 lb Side Load



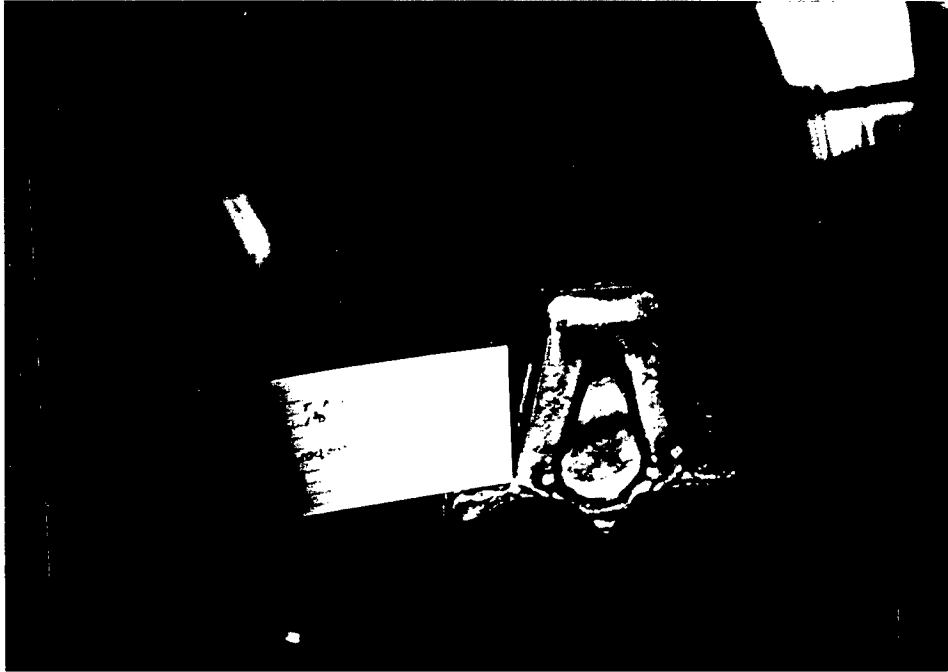
T-158 (final design) Assembly Stress Distribution



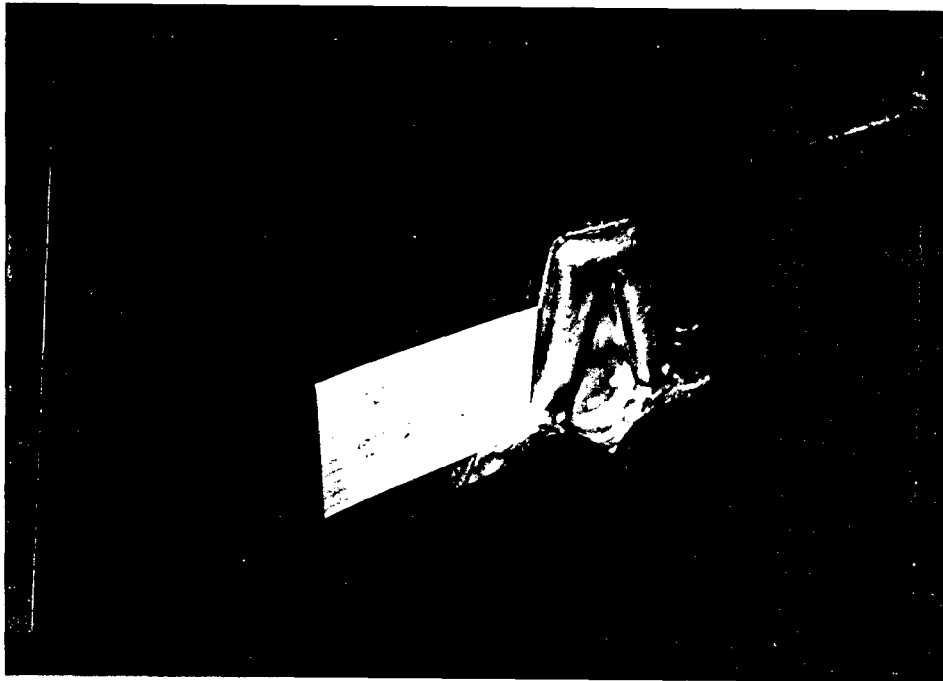
T-158 (final design) Stress Distribution at 60,000  
lb Tensile Load



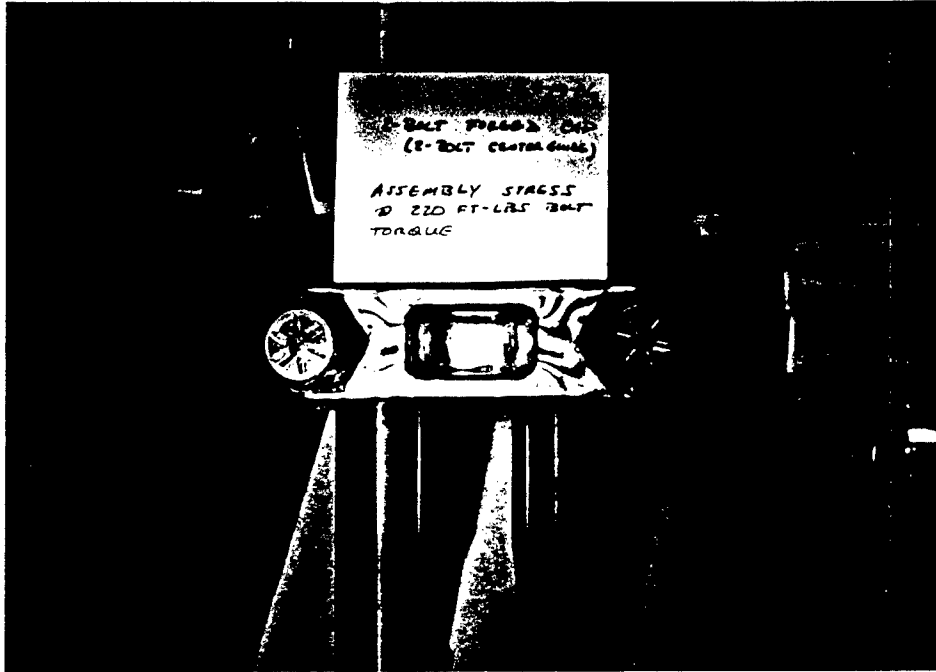
T-158 (final) Stress Distribution at 60,000  
lb Tensile and 6,000 lb Side Load (12,000 lb  
load shown on card is shared by 2 centerguides)



T-158 (final) Stress Distribution at 100,000  
lb Tensile Load



T-158 (final) Stress Distribution at 100,000  
lb Tensile and 6,000 lb Side Load (12,000 lb  
load shown on card is shared by 2 centerguides)



T-158 Cap Assembly Stress Distribution (no load)

APPENDIX C

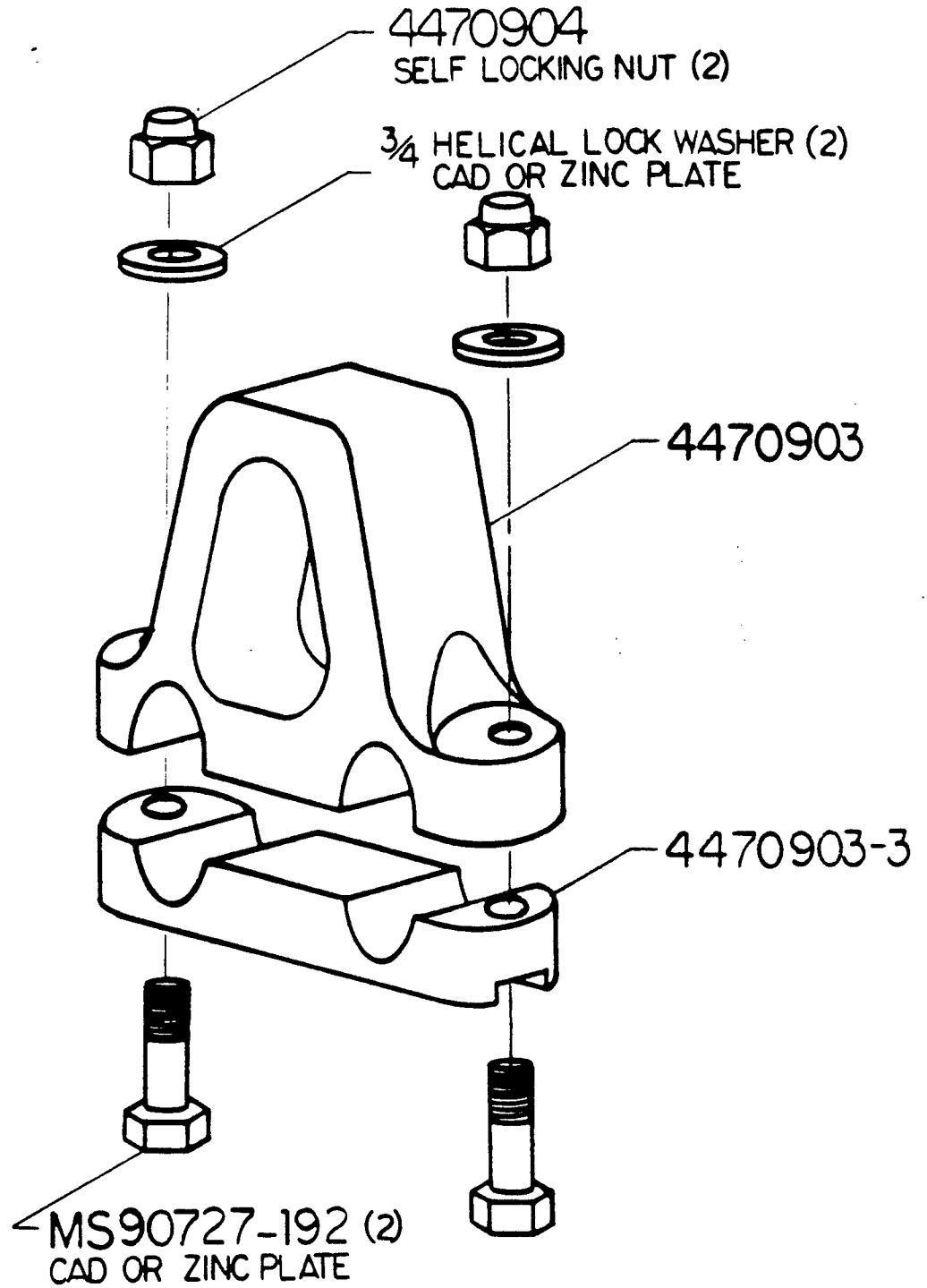
GENERAL REFERENCE INFORMATION







# T-158 CENTER GUIDE PN 4470903



# Full-Field Interpretation of Photoelastic Fringe Patterns

## 1.0 INTRODUCTION

In addition to its many uses in making accurate strain measurements at preselected test points by the procedures described in the following Parts, the 030-series polariscope provides another equally important capability to the stress analyst. This is the facility for immediate recognition of nominal strain (and stress) magnitudes, strain gradients, and overall strain distribution — including identification of overstressed and understressed areas. This extremely valuable attribute of the PhotoStress<sup>®</sup> method, described as full-field interpretation, is unique to photoelastic methods of stress analysis. Its successful application depends only on the recognition of isochromatic fringe orders by color, and an understanding of the relationship between fringe order and strain magnitude.

Aside from its colorful and often esthetically pleasing character, the photoelastic fringe pattern is rich with information and insights for the design engineer. If, for example, a part is being stress analyzed with photoelastic coating as a result of field service failures, the overall photoelastic pattern will usually suggest corrective measures for preventing the failures — often involving material removal and weight reduction. Because of the full-field picture of stress distribution seen by the polariscope user, he may note that the overstressed zone responsible for the failures is surrounded by an area of near zero stress; and a slight change in shape will redistribute the stresses so as to eliminate the stress concentration, while forcing the understressed material to carry its share of the load.

Similarly, in prototype stress analysis for product development purposes, the photoelastic pattern will point the way toward design modifications to achieve the minimum-weight, functionally adequate part — i.e., the optimum design. In addition, full-field observation of the stress distribution easily shows the effects of varying modes of loading, as well as the relative significance of individual loads and/or load directions. These examples are merely indicative of the many ways in which full-field fringe patterns in photoelastically coated test parts speak out to the knowledgeable stress analyst and provide him with comprehension not achievable from "blind" strain measurements at a point.

In Section 2 the relationships are given for determining the strain and stress magnitudes from the fringe orders. The practical application of these relationships does not require familiarity with photoelastic theory or the optics of a polariscope.\* On the other hand, acquaintance with elementary mechanics (or "strength") of materials will contribute noticeably to the information extractable from a quick study of the overall fringe pattern.

Full-field interpretation of photoelastic patterns requires that the observer be able to identify fringe orders by color. This art can be learned quickly with a little practice; and Section 3 provides all of the information needed to do so.

Section 4 demonstrates the application of the principles in Sections 2 and 3 to actual stress analysis, and gives some of the "tricks of the trade" — that is, generally unpublished methods often used by professionals in the overall interpretation of fringe patterns.

\*For background reference as needed, these topics are developed in Part IPH of this manual. The same topics are treated more comprehensively in the textbooks and other references listed in the Bibliography (see Appendix).

## 2.0 RELATIONSHIPS BETWEEN FRINGE ORDERS AND MAGNITUDES OF STRAIN AND STRESS

When a photoelastically coated test object is subjected to loads, the resulting stresses cause strains to exist generally throughout the part and over its surface. The surface stresses and strains are commonly the largest, and of the greatest importance. Because the photoelastic coating is intimately and uniformly bonded to the surface of the part, the strains in the part are faithfully transmitted to the coating. The strains in the coating produce proportional optical effects which appear as *isochromatic fringes* when viewed with a reflection polariscope (see Part IPH).

Starting with the unloaded test part, and applying the load or loads in increments, fringes will appear first at the most highly stressed points (Fig. 1, following page). As the load is increased and new fringes appear, the earlier fringes are pushed toward the areas of lower stress. With further loading, additional fringes are generated in the highly stressed regions and move toward regions of zero or low stress until the maximum load is reached. The fringes can be assigned ordinal numbers (first, second, third, etc.) as they appear, and they will retain their individual identities ("orders") throughout the loading sequence. Not only are fringes *ordered* in the sense of serial numbering, but they are also *orderly* — i.e., they are continuous, they never cross or merge with one another, and they always maintain their respective positions in the ordered sequence.

The fringe orders observed in photoelastic coatings are proportional to the difference between the principal strains in the coating (and in the surface of the test part). This simple linear relationship is expressed as follows:

$$\epsilon_x - \epsilon_y = f \cdot N \quad (1)$$

where:  $\epsilon_x, \epsilon_y$  = principal strains in coating and part surface

$f$  = fringe value of coating (obtained by calibrating the coating)

$N$  = fringe order — observed birefringence, expressed in fringe units

Equation (1) can also be written in terms of shear strain,  $\gamma_{xy}$ :

$$\gamma_{xy} = f \cdot N \quad (2)$$

where:  $\gamma_{xy}$  = maximum shear strain (in the plane of the part surface) at any point

The significance of the preceding is that the difference in the principal strains, or the maximum shear strain in the surface of the test part, can be obtained by simply recognizing the fringe order in the coating and multiplying by the fringe value of the plastic.

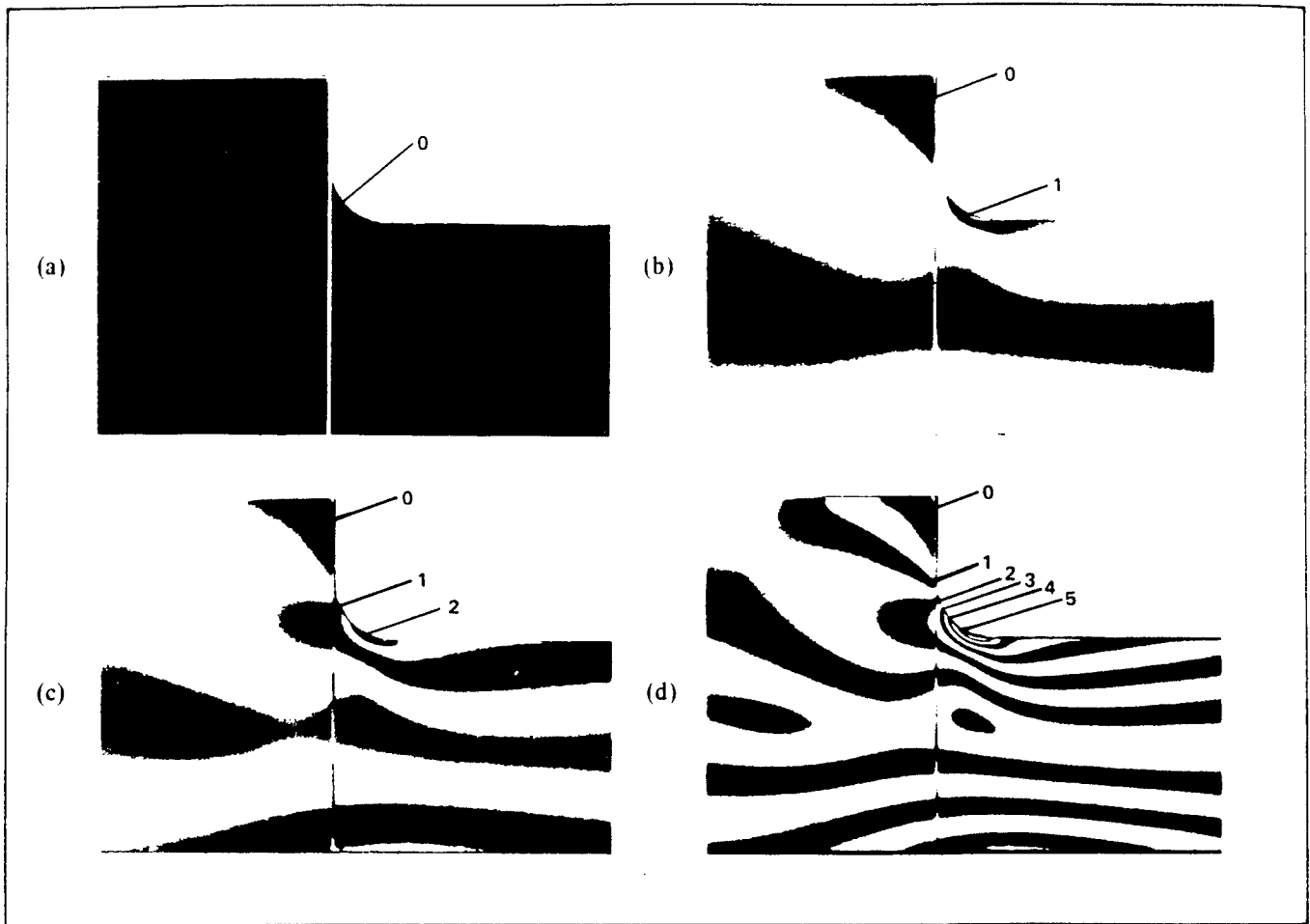


Fig. 1 – Fringe generation at a fillet in bending: (a) no load (zero-order fringe covers the specimen); (b), (c), and (d) increasing load and fringe order in the fillet.

Engineers and designers often work with stress rather than strain; and, for this purpose, Eqs. (1) and (2) can be transformed by introducing the biaxial Hooke's law:

$$\sigma_x = \frac{E}{1-\nu^2} (\epsilon_x + \nu\epsilon_y) \quad (3)$$

$$\sigma_y = \frac{E}{1-\nu^2} (\epsilon_y + \nu\epsilon_x) \quad (4)$$

and,

$$\sigma_x - \sigma_y = \frac{E}{1+\nu} (\epsilon_x - \epsilon_y) \quad (5)$$

Substituting Eq. (1) into Eq. (5),

$$\sigma_x - \sigma_y = \frac{E}{1+\nu} fN \quad (\text{see footnote below}) \quad (6)$$

where:  $\sigma_x, \sigma_y$  = principal stresses in test part surface

$E$  = elastic modulus of test part

$\nu$  = Poisson's ratio of test part

For convenient reference, approximate values of the factor  $E/(1+\nu)$  for several structural materials are as follows:

Steel –  $23.5 \times 10^6$  psi; 162 GPa

Aluminum alloy –  $7.90 \times 10^6$  psi; 54.5 GPa

Magnesium –  $4.80 \times 10^6$  psi; 33.1 GPa

And, noting that the maximum shear stress,  $\tau_{max}$ , in the plane of the surface at any point is  $(\sigma_x - \sigma_y)/2$ ,

$$\tau_{max} = \frac{1}{2} \left( \frac{E}{1+\nu} \right) fN \quad (7)$$

Equations (1) and (6), which are the primary relationships used in photoelastic coating stress analysis, give only the difference in principal strains and stresses, not the individual quantities. To determine the individual magnitudes and signs of either the principal strains or stresses generally requires, for biaxial stress states, a second measurement of fringe order in oblique incidence (Part SPS). There are many cases, however, when these equations provide all of the information needed for stress analysis. For instance, when the ratio of principal stresses can be inferred from other considerations – a uniform shaft in torsion ( $\sigma_x/\sigma_y = -1$ ), a thin-walled pressure vessel ( $\sigma_x/\sigma_y = 2$ ), etc. – this relationship can be combined with Eq. (6) to solve for the individual principal stresses. And, whenever the stress state is known to be uniaxial, with either  $\sigma_x$  or  $\sigma_y$  being zero, there is only one nonzero principal stress in the plane of the test part surface, and this can be obtained directly from Eq. (6). For example, if  $\sigma_y = 0$ ,

$$\sigma_x = \frac{E}{1+\nu} fN \quad (8)$$

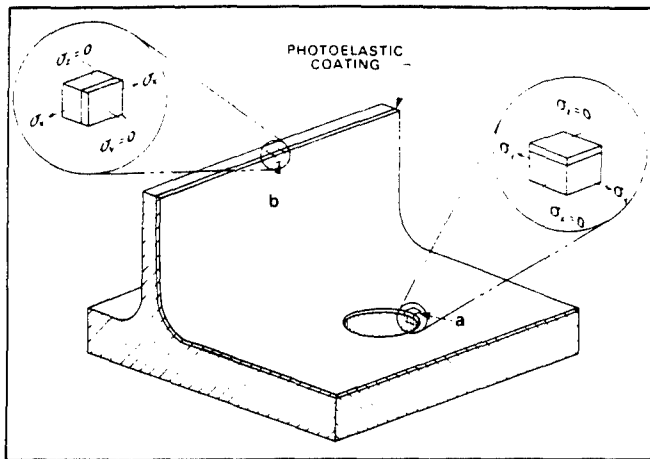


Fig. 2 – Section from a coated test member showing uniaxial stress states on free edges.

The cases in which one of the principal surface stresses is zero include all straight, uniform-cross-section members in axial tension or compression (and bending), away from points of load application. Even for mildly tapered members, so loaded, the stress state is very nearly uniaxial, and Eq. (8) can often be applied as a very good approximation. A much more important class of cases from the viewpoint of practical stress analysis involves all points on the boundaries and free edges of the test part.

Consider, for example, an unloaded hole penetrating the test part. At every point on the edge of the hole the principal axes are normal and tangential, respectively, to the edge. Because the principal stress normal to the edge is necessarily zero, the stress state is uniaxial, and the only nonzero principal stress is everywhere tangent to the hole edge. There are many other cases, such as projecting flanges and ribs, and "two-dimensional" objects in general, in which the stress state on the unloaded edge is always uniaxial. For all such cases, the single nonzero principal stress, which is tangent to the edge, can be determined directly from the observed fringe order by substituting into Eq. (8); or, in effect, multiplying the fringe order by a constant.

Figure 2 shows a portion of the surface of a steel machine part to which a photoelastic coating has been applied. As indicated, the coating has been finished to accurately match the edge of the hole and that of the rib. The uniaxial stress state at points *a* and *b* is demonstrated by the enlarged free-body diagrams of elements of matter removed from the edges for examination. With the part under normal service loading, and viewing the coating with the O30-series polariscope, a fringe order of 2 is observed at point *a*, and about 3/4 at point *b*. Previous calibration has established a fringe value of 1100  $\mu\epsilon$  per fringe for this coating. Thus, the stress at point *a* in the more critical region can be calculated directly from Eq. (8), using the information from the footnote on page FFI-2:

$$\sigma_x = 23.5 \times 10^6 \times 1100 \times 10^{-6} \times 2 = 51\,700 \text{ psi}$$

or,

$$\sigma_x = 162 \times 10^9 \times 1100 \times 10^{-6} \times 2 = 356 \text{ MPa}$$

And similarly, the stress at the edge of the rib is about 19 400 psi, or 134 MPa.

Summarizing this section, the difference between principal strains can be determined from Eq. (1), and the difference between principal stresses from Eq. (6), at any point on a photoelastically coated surface. At points where the stress state is uniaxial, Eq. (8) gives the principal stress directly. In each case, the result is obtained by multiplying the observed fringe order by a constant. It remains, then, only to identify the fringe order. Techniques for accomplishing this by direct observation are described in the following section.

### 3.0 IDENTIFICATION OF FRINGE ORDERS

Under white light, the photoelastic fringe pattern appears as a series of successive and contiguous different-colored bands (isochromatics) in which each band represents a different degree of birefringence corresponding to the underlying strain in the test part. Thus, the color of each band uniquely identifies the birefringence, or fringe order (and strain level), everywhere along that band. With an understanding of the unvarying sequence in which the colors appear, the photoelastic fringe pattern can be read much like a topographical map to visualize the stress distribution over the surface of the coated test part.

The photoelastic effect is described in Part IPH in terms of monochromatic light for simplicity of explanation. It is shown there that the fringe pattern is caused by alternately constructive and destructive interference between light rays which have undergone relative retardation, or phase shift, in the stressed photoelastic model or coating. When, in a dark-field polariscope, the magnitude of the relative retardation is an integral multiple of the wavelength ( $\lambda$ ,  $2\lambda$ ,  $3\lambda$ , etc.), the rays are 180 degrees out of phase, and there is mutual cancellation, causing extinction of the light and producing a black band. On the other hand, when the relative retardation is an odd multiple of  $\lambda/2$  ( $\lambda/2$ ,  $3\lambda/2$ ,  $5\lambda/2$ , etc.), the rays are perfectly in phase and combine to cause maximum brightness. Intermediate magnitudes of relative retardation produce intermediate light intensities. However, because the light intensity is a sine-squared function of the relative retardation, the resulting photoelastic pattern appears to be made up of alternate light and dark fringes.

White light, generally used for full-field interpretation of fringe patterns in photoelastic coatings, is composed of all wavelengths in the visible spectrum. Thus, the relative retardation which causes extinction of one wavelength (color) does not generally extinguish others. When, with increasing birefringence, each color in the spectrum is extinguished in turn according to its wavelength (starting with violet, the shortest visible wavelength), the observer sees the complementary color. It is these complementary colors which make up the visible fringe pattern in white light. The complete color sequence is given in Table 1 (page FFI-5), including, for each color, the relative retardation, the numerical fringe order, and the corresponding strain level in a typical coating.

The O30-series polariscope is a dark-field instrument, which means that with no stress in the coated test object, and therefore no strain-induced birefringence in the coating, all light is extinguished and the coating appears uniformly black. As load is gradually applied to the specimen, the most highly stressed region begins to take on color—first gray, then white; and, when the violet is extinguished, yellow. With further load, the blue is extinguished to produce orange; and then green, to give red. The next color to vanish with increasing load is yellow, leaving a purple color; and this is followed by the extinction of orange, producing a deep blue fringe.

The purple fringe, which is easily distinguished from the red and blue on either side, and is very sensitive to a small change in strain level, is referred to as the *tint of passage*. Because of its distinctiveness and resolution, the purple tint of passage is selected to mark the increment in relative retardation equal to a fringe order of unity ( $N = 1$ ).<sup>1</sup> Subsequent recurrence of the tint of passage with greater relative retardation signifies the presence of higher integral fringe orders ( $N = 2, N = 3$ , etc.).

Continuing to increase the load on the test specimen and producing additional relative retardation, the red is extinguished from the white light spectrum, and the fringe color is blue-green. With still greater load, the relative retardation reaches the point where it corresponds to twice the wavelength of violet, extinguishing this color for the second time and starting the fringe cycle over again. However, the deep red color at the far end of the white light spectrum also has twice the wavelength of violet, and thus undergoes its first extinction simultaneously with the second extinction of violet. The result is that the fringe color is the combination of two complementary colors, yellow and green. As the load and relative retardation continue to increase, the fringe color cycle is repeated, but the colors are not exactly the same as in the first cycle because of simultaneous extinction of two or more colors. With each successive complete color cycle the effect of increasingly complex simultaneous extinctions is to cause the fringe colors to become paler and less distinctive. Because of this effect, fringe orders above 4 or 5 are not distinguishable by color in white light. Although fringe orders higher than 3 are rarely encountered (or needed) in stress analysis with photoelastic coatings, fringes of very high order can always be detected with monochromatic light.

Because of simultaneous multiple extinction of colors, the second-order tint of passage is fainter than the first, and falls in the transition area between red and green fringes. At fringe orders of 3 and 4 the tint of passage is not distinctly visible as a purple band, but the well-defined transition between red and green in each case serves the same function and represents the integral fringe order.

The ability to identify integral and fractional fringe orders by color depends primarily upon intimate familiarity with the fringe colors and the sequence in which they always appear. Such familiarity is obtained only by practice and drill. For this purpose, the following exercises are strongly recommended.

Prepare an aluminum-alloy cantilever beam,  $\frac{1}{4} \times 1 \times 12\frac{1}{2}$  in (approximately  $6 \times 25 \times 300$  mm), for analysis by coating the beam on one side with Photolastic plastic, Type PS-1, 0.080 in (2 mm) thick, leaving one end uncoated for mounting the beam.<sup>2</sup> Mount the beam in the Model 010-B Calibrator, or clamp it to the edge of a workbench (coated side up) so that the coated portion of the beam overhangs the edge of the bench.

Set up the 030 polariscope for normal-incidence viewing of the coated beam surface (Fig. 3). Set the COMPENSATOR ring on the analyzer at zero, and move knob "B" to the M (magnitude) position. Make certain that the beam is illuminated by the light coming from the instrument (partial darkening of a very bright room will make the colors somewhat easier to distinguish, but is not ordinarily necessary). Load the beam sufficiently to produce at least three fringes.

<sup>1</sup> The tint of passage corresponds to a full wavelength of relative retardation for a wavelength of 575 nm. This wavelength is at the center of the  $\pm 5$  nm bandpass of the Photolastic Model 036 interference monochromator. As a result, there is no fringe shift or change in apparent fringe order whether the coating is viewed or photographed through the polariscope with white light or with monochromatic light.

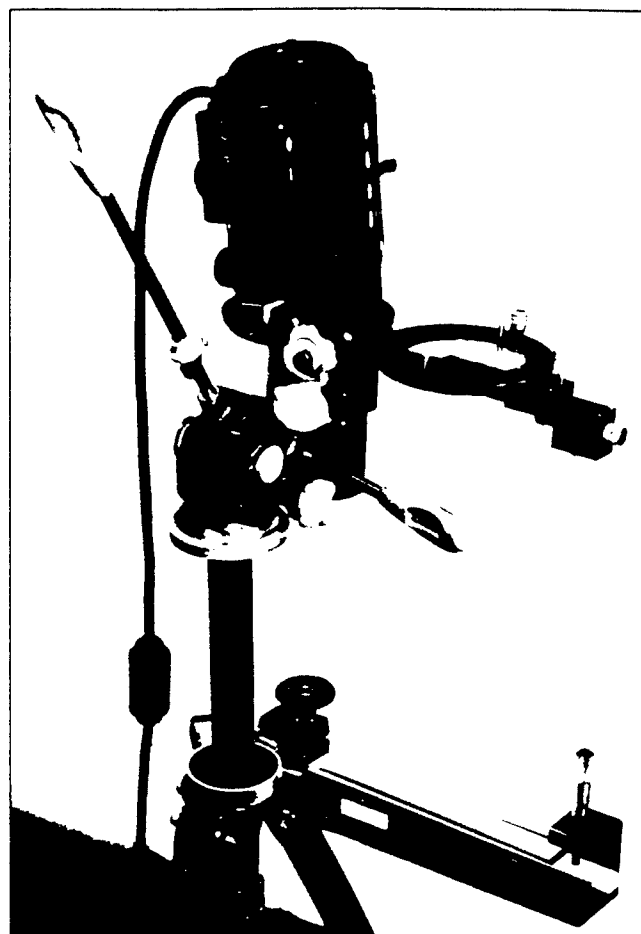


Fig. 3 - Coated cantilever beam mounted in Model 010-B Calibrator for fringe identification exercise.

Study the colored fringe pattern along the beam, and compare the color sequence to those in TABLE 1 and Fig. 4 (allowing, in the latter case, for the inadequacies in the printed reproduction of color). Note that in a cantilever beam the bending stress varies linearly from zero at the point of load application to a maximum at the clamped end. The fringe colors in the coating should vary correspondingly, progressing as follows: black, yellow, red, purple, blue, yellow, red, purple, blue-green, yellow-green, red, green. The first integral-order fringe occurs at the purple tint of passage between the red and blue, the second fringe at the fainter purple between red and blue-green, and the third at the transition between red and green. With a grease pencil, mark a cross on the centerline of the beam at each integral fringe order. Notice that if the marks are correctly located, the distance between the point of load application and the mark for  $N = 1$  is the same as the distance from  $N = 1$  to  $N = 2$ , and from  $N = 2$  to  $N = 3$  - demonstrating the linear stress distribution in the beam.

<sup>2</sup> Note: For best results in this exercise, the ambient temperature while observing the fringe pattern should (ideally) be the same as that during application of the coating to the beam. Because of the difference in thermal expansion coefficients between the aluminum beam and the coating, a change in temperature between application of the coating and observation of the fringe pattern will cause "parasitic" birefringence to exist everywhere along the edge of the beam. For instance, a  $10^\circ\text{F}$  ( $5^\circ\text{C}$ ) change in temperature will result in about 1/3 fringe at the beam edge for a typical coating. Although this effect can easily be corrected for in practical stress analysis (see Part COR), the presence of the parasitic birefringence detracts from the purity of this exercise. For example, the lower-order fringes may curve near the edges instead of forming straight bands of color across the beam. Should this occur, the fringe identification should be made at the center of the beam, where the temperature effect does not exist.

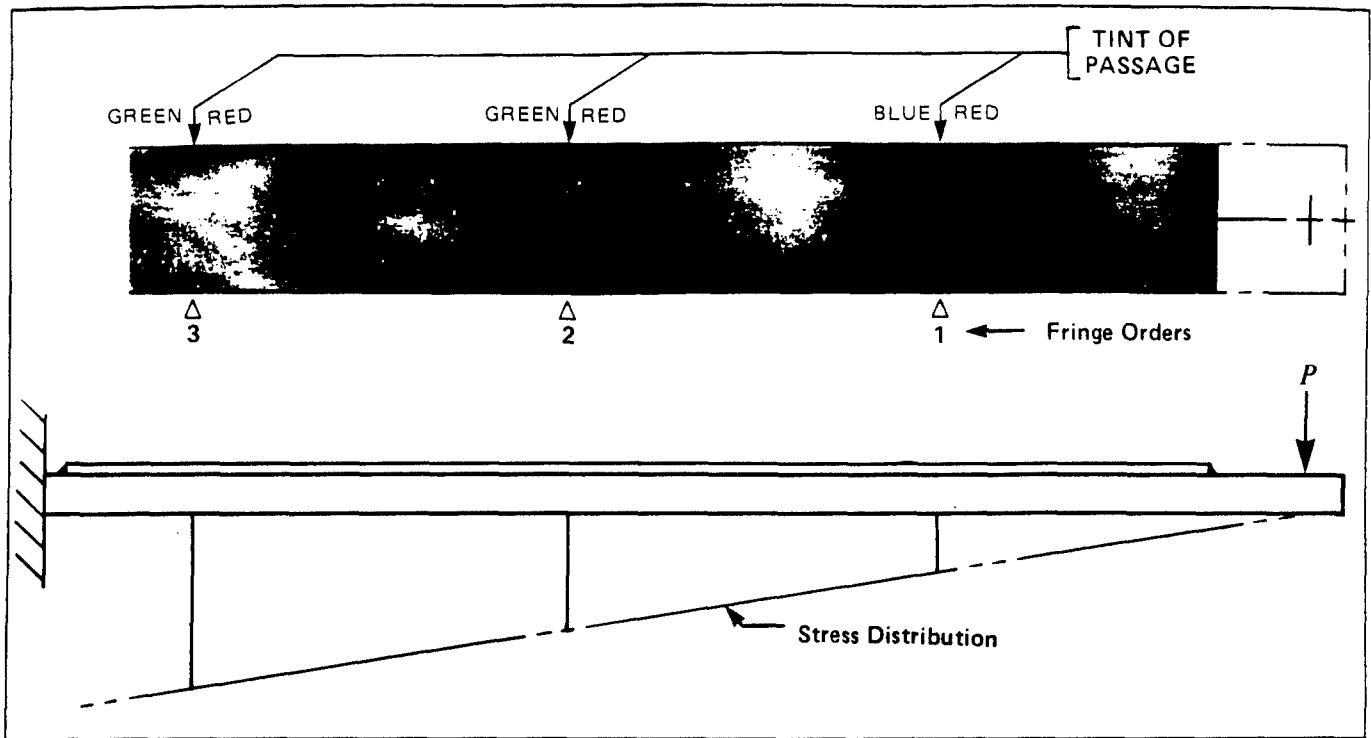


Fig. 4 – Fringe color sequence on a coated cantilever beam.

For future application in full-field interpretation of fringe patterns, notice also the pale yellow at about  $N = 1/2$ , and the orange at  $N = 3/4$ . Erase the marks and repeat the procedure as necessary until the integral fringe orders can be located with consistent accuracy.

A limitation of the cantilever beam exercise is that some of the color bands listed in Table 1 are not readily visible because the colors along the beam blend continuously from one to the next. A second exercise will permit seeing sizeable expanses of individual colors, one at a time. This can be accomplished by the following procedure.

Remove all load from the beam. When viewed through the analyzer of the polariscope the coating should be uniformly black or dark gray except, perhaps, along the edges. Install the Model 232 Null-Balance Compensator on the analyzer assembly (see Part NBC), and set the digital register of the compensator on zero. Relocate the polariscope with respect to the beam as necessary so that the coating is viewed through the compensator window with no parallax between the eye and the window – i.e., along a normal to the window surface. So viewed, the coating should have the same appearance as when viewed through the analyzer alone.

The complete sequence of fringe colors can now be observed, color-by-color, by turning the counter knob on the compensator. Using the compensator calibration curve to determine the fringe order for any counter setting (and vice versa), the colors can be correlated directly with Table 1. For instance, adjust the compensator for a setting equivalent to  $N = 0.5$ . A pale yellow fringe will cover the coating. Now, in order, set the compensator at counter readings corresponding to  $N = 0.6, 0.75, 0.9$ , and  $1.0$ ; and produce, respectively, bright yellow, orange, red, and purple (the tint of passage). At this point, adjust the compensator slowly back and forth between the deep red and violet-blue until the color of the tint of passage in contrast to the neighboring colors is thoroughly impressed on the memory.

TABLE 1  
Isochromatic Fringe Characteristics

Color	Approximate Relative Retardation nm	Fringe Order N	Strain* $\mu\epsilon$
BLACK	0	0	0
GRAY	160	0.28	265
WHITE	260	0.45	425
PALE YELLOW	345	0.60	570
ORANGE	460	0.80	760
DULL RED	520	0.90	855
PURPLE (TINT OF PASSAGE)	575	1.00	950
DEEP BLUE	620	1.08	1025
BLUE-GREEN	700	1.22	1160
GREEN-YELLOW	800	1.39	1320
ORANGE	935	1.63	1550
ROSE RED	1050	1.82	1730
PURPLE (TINT OF PASSAGE)	1150	2.00	1900
GREEN	1350	2.35	2230
GREEN-YELLOW	1440	2.50	2380
RED	1520	2.65	2520
RED/GREEN TRANSITION	1730	3.00	2850
GREEN	1800	3.10	2950
PINK	2100	3.65	3470
PINK/GREEN TRANSITION	2300	4.00	3800
GREEN	2400	4.15	3940

\*Type PS-1 Photoelastic Plastic, 0.080 in (2 mm) thick,  
 $f = 950 \mu\epsilon/\text{fringe (reflection)}$

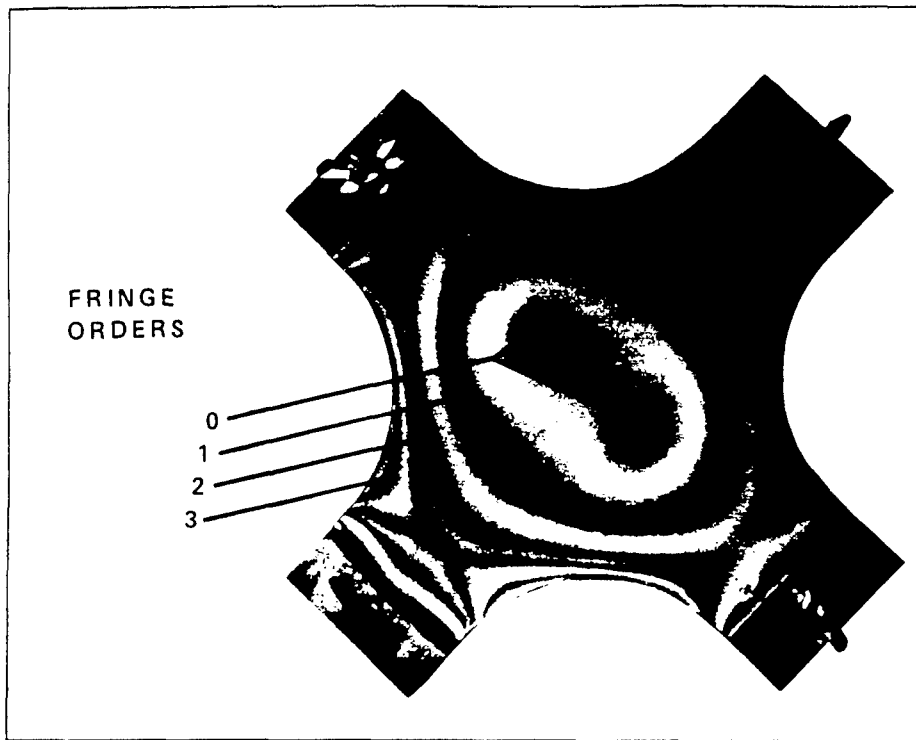


Fig. 5 – Fringe pattern on a coated demonstration specimen in biaxial bending.

Continue adding relative retardation with the compensator to display the colors corresponding to higher fringe orders. Notice particularly the fringe appearance at  $N = 2$ , and the transition between red, or pink, and green which marks the integral fringe order for  $N = 3$  and  $N = 4$ .

When analyzing coated test objects under load, many of the individual colors in Table 1 will not be seen, particularly in regions of high strain gradient, because the color bands are very narrow, and blend continuously. For practical interpretation of overall fringe patterns, Table 1 can be reduced to only the more dominant colors as listed in Table 2.

TABLE 2  
Dominant Isochromatic Fringe Colors  
for Full-Field Interpretation

Color	Approximate Fringe Order
BLACK	0
YELLOW	0.6
RED	0.9
PURPLE (TINT OF PASSAGE)	1.0
BLUE-GREEN	1.2
YELLOW	1.5
RED	1.75
RED/GREEN TRANSITION	2.0
GREEN	2.2
YELLOW	2.5
RED	2.8
RED/GREEN TRANSITION	3.0
GREEN	3.2

#### 4.0 FULL-FIELD ANALYSIS OF PHOTOELASTIC PATTERNS

The two preceding sections have provided all of the background necessary to: (a) identify fringe orders, and (b) determine the difference in principal stresses (and, on free boundaries, the only principal stress) from the fringe orders. With these tools, and some familiarity with elementary mechanics of materials, the polariscope user can understand a great deal about the stress distribution in a coated part by direct observation of the fringe pattern.

Photoelastic fringes have characteristic behaviors which are very helpful in fringe pattern interpretation. For instance, the fringes are ordinarily continuous bands, forming either closed loops or curved lines, which originate and terminate on boundaries. The black zero-order fringes are usually isolated spots, lines, or areas surrounded by or adjacent to higher-order fringes. The fringes never intersect, or otherwise lose their identities, and therefore the fringe order and strain level are uniform at every point on a fringe. Furthermore, the fringes always exist in a continuous sequence by both number and color. In other words, if the first- and third-order fringes are identified, the second-order fringe must lie between them. The color sequence in any direction establishes whether the fringe order and strain level increase or decrease in that direction. From Table 2 it can be seen that the sequence yellow-red-green-yellow-red-green corresponds to increasing strain level; and, of course, the opposite sequence, green-red-yellow-green-red-yellow, indicates decreasing strain. It is important to memorize the association between the color sequence and the sign of the strain gradient so that directions of increasing and decreasing levels are obvious by inspection.

It turns out that the characteristics of photoelastic fringes mentioned in the preceding paragraph are the same as those of constant-level contours on a colored topographic map. As a result, any photoelastic pattern can be considered, and visualized, as a contour map of the difference (without regard to sign) between principal strains or stresses over the

surface of the test part. In other words, the magnitudes of the strain levels, as indicated by the fringe orders, correspond directly to constant-altitude levels on a topographic map. And the fringe pattern depicts peaks and valleys, plains and mesas — with "sea level" represented by the zero-order fringes.

Figure 5 is the photoelastic pattern (with fringes identified) on a coated demonstration specimen in biaxial bending. Although the coating in this instance is characterized by an amber cast which filters some of the bright colors, the photograph clearly shows two black zero-order spots in the central area where the difference in principal strains (and stresses) is zero. Then, as indicated by the labeled fringe-order contours, the strain level can be seen to rise in the directions of the loading arms. Notice that in the direction of rising fringe order the pattern exhibits the color sequence yellow-red-green, etc., and vice versa. It can also be seen that the fringes become narrower and draw closer together where the strain gradient is steep (approaching the large scallops, for instance), and widen and separate in regions of low gradient such as the central area.

Where stress concentration exists — for example, at a fillet, hole, or notch — the fringes usually form a locally confined pattern of tightly grouped loops because the strain gradient is so steep. On the other hand, when a single uniform color covers a large area, it indicates unvarying strain throughout the area. For instance, in a perfectly aligned tensile specimen of uniform cross section, the entire surface of the coated specimen will exhibit a single color (away from points of load application).

The first step in interpreting a fringe pattern is to locate one or more prominently displayed or otherwise obvious fringe orders which can be identified without ambiguity. The stress analyst then departs from these, following the variation in fringe order to other points of interest. The procedure is quite analogous to the use of a map: i.e., one first locates a recognizable city or geographic feature and uses this as a point of departure from which to study other locations.

If there is a zero-order fringe in the field of view, it will usually be obvious by its black color. Assuming that the coated test part has a free square corner or pointed projec-

tion, the stress there will always be zero, and a zero-order fringe (spot) will exist in the corner, irrespective of the load magnitude, but shrinking in size slightly as the load increases. When there is no zero-order fringe evident, the first-order fringe can often be recognized because of the bright colors adjacent to the purple tint of passage. As an alternative, when the test object can be loaded incrementally from an initially stress-free state, the starting zero-order fringe which covers the entire coating can usually be followed throughout the loading process as it recedes toward unstressed points, and regions where the difference in principal stresses is zero.

Once one fringe has been identified, orders can be assigned to the other fringes, making certain that the direction of increasing fringe order corresponds to the correct color sequence — i.e., yellow-red-green, etc. By this process the observer can quickly locate the highest fringe orders and, generally, the most highly strained regions. Areas of closely spaced fine fringes will usually attract his attention, since regions of steep strain gradient ordinarily signify high strains as well. The stress analyst will also note any large areas where the pattern is almost uniformly black or gray, indicating a significantly understressed region.

Frequently, the process of locating the highest fringe orders will lead the observer to one or more critical points on a free boundary. When this occurs, the stress analyst knows that the single principal stress at such a point is tangent to the boundary, and its magnitude can be obtained directly by multiplying the fringe order by a constant [Eq. (8)]. The sign of the stress, plus or minus for tension or compression, can also be determined very easily on a free boundary. This is done by pushing gently on the edge of the photoelastic coating with a sharp object such as a ballpoint pen. If the fringe nearest the boundary bulges in the direction of increasing fringe order, the boundary stress is compressive. Correspondingly, a tensile boundary stress will cause the fringe to bulge in the direction of decreasing fringe order. Should there be any doubt about the sign of the boundary stress, it can always be determined rigorously with compensation methods as described in Parts NBC and TDC.

DISTRIBUTION LIST

	Copies
Commander U. S. Army Tank-Automotive Command ATTN: AMSTA-TMS Warren, MI 48397-5000	1
Commander U. S. Army Tank-Automotive Command ATTN: AMSTA-RCKT Warren, MI 48397-5000	12
Commander U. S. Army Tank-Automotive Command ATTN: AMSTA-IRDA Warren, MI 48397-5000	1
Commander U. S. Army Tank-Automotive Command ATTN: ACO Warren, MI 48397-5000	1
Commander U. S. Army Tank-Automotive Command ATTN: AMSTA-DDL Warren, MI 48397-5000	2
Commander Defense Technical Information Center Bldg. 5, Cameron Station ATTN: DDAC Alexandria, VA 22314	12
Manager Defense Logistics Studies Information Exchange ATTN: AMXMC-D Fort Lee, VA 23801-6044	2
Commander U. S. Army Tank-Automotive Command ATTN: AMSTA-CF (Mr. Orlicki) Warren, MI 48397-5000	1